ATLAS NOTE

ATLAS-CONF-2012-097

July 6, 2012

Measuring the b-tag efficiency in a $t\bar{t}$ sample with 4.7 fb^{-1} of data from the ATLAS detector

The ATLAS Collaboration

Abstract

Many physics analyses in ATLAS depend on the reconstruction of b-jets. Aside from reliable b-tagging algorithms, an appropriate description of the b-tagging efficiencies based on measurements with data is essential for correctly modelling the measurements in Monte Carlo simulation. Furthermore, the systematic uncertainties need to be estimated realistically. Since many analyses at a centre of mass energy of $\sqrt{s} = 7$ TeV include high p_{T} jets, it is desirable to calibrate the b-tagging algorithms at comparable jet energies. With the large data sample collected in 2011 of 4.7 fb^{-1}, new calibration methods based on $t\bar{t}$ events have been developed. The measurements of the b-tagging efficiency are provided in the form of jet p_{T} dependent scale factors that correct the b-tagging performance in simulation to that observed in data. For all b-tagging algorithms calibrated, the scale factors measured with the various $t\bar{t}$ based methods are in good agreement with each other. The total uncertainties range from 5% to 15% for jet p_{T} in the range 25 GeV to 300 GeV.

ATLAS-CONF-2012-097
09 July 2012

1 Introduction

The identification of b-jets is of great importance in many physics analyses at the LHC. The performance of b-tagging algorithms has to be validated using data, as the Monte Carlo simulation does not fully describe the performance of the detector. The calibration of b-tagging algorithms includes the measurement of the mis-tag rates and b-tagging efficiency.

The main b-tagging efficiency calibration methods used so far, the so called system8 and $p_{\mathrm{T}}^{\mathrm{rel}}$ methods, are described in detail in [1] based on an integrated luminosity of $\mathcal{L} = 4.7\,\mathrm{fb}^{-1}$ collected in 2011. These measurements are based on a sample of jets with muons inside, where the muons are serving as a reference b-tagging algorithm to obtain a b-jet sample on which the calibrations can be performed. At the LHC, the large $t\bar{t}$ production cross section of $\sigma_{t\bar{t}} = 177 \pm 3(\mathrm{stat.})^{+8}_{-7}(\mathrm{sys.}) \pm 7(\mathrm{lum.})\,\mathrm{pb}$ [2] offers an alternative source of events enriched in b-jets. This distinctive topology with high p_{T} leptons, multiple jets, and large missing transverse momentum provides highly selective trigger objects and is relatively easy to reconstruct. With the large integrated luminosity of $4.7\,\mathrm{fb}^{-1}$ collected during 2011, the methods based on $t\bar{t}$ selections have become competitive for the first time. In addition to providing b-tagging calibration measurements in an inclusive b-jet sample rather than a sample of semileptonic b-jets, these methods also allow to extend the calibrated p_{T} range. Furthermore, the $t\bar{t}$ environment of high jet multiplicity and high p_{T} b-jets is more similar to the final states to which b-tagging is applied than the semileptonic jet sample.

This note presents analyses performed with three different methods using two statistically independent selections of $t\bar{t}$ events according to the single lepton and dilepton decay modes of top quark pairs. Applying the same calibration method to the two independent data selections and to calibrate the same data selection with different, independent methods is an essential cross check to ensure the reliability of the individual calibration analyses. The results of all calibration methods are presented in the form of p_{T}-dependent scale factors $\kappa_{\varepsilon_b}^{\mathrm{data/sim}}$, defined as

$$\kappa_{\varepsilon_b}^{\mathrm{data/sim}}(p_{\mathrm{T}}) = \frac{\varepsilon_b^{\mathrm{data}}(p_{\mathrm{T}})}{\varepsilon_b^{\mathrm{sim}}(p_{\mathrm{T}})}, \tag{1}$$

where $\varepsilon_b^{\mathrm{sim}}$ is the fraction of b-jets which are tagged in simulated events, with the jet flavour defined by matching to generator level partons. In physics analyses, these p_{T}-dependent scale factors are then applied as weights to the jets in Monte Carlo simulation, to reproduce the b-tagging performance measured in data.

2 Data, simulated samples and top quark pair reconstruction

2.1 Monte Carlo samples

The $t\bar{t}$ signal is simulated using MC@NLO v3.41 [3] with the mass of the top quark set to 172.5 GeV and with the cross section normalised to the approximate NNLO calculation from Hathor 1.2 [4] using the MSTW 2008 50% PDF sets [5], incorporating PDF+α_S uncertainties according to the MSTW prescription [6] cross checked with the approximate NNLO calculation of Cacciari et al. [7] as implemented in Top++1.0 [8]. For the main backgrounds, which consist of W/Z boson production in association with multiple jets, ALPGEN v2.13 [9] is used, which implements the exact LO matrix elements for final states with up to six partons. Using the LO PDF set CTEQ6L1 [10], the following backgrounds are generated: W+jets events with up to five partons, Z/γ^*+jets events with up to five partons and with the dilepton invariant mass $m_{\ell\ell} > 40$ GeV and diboson WW+jets, WZ+jets and ZZ+jets events. A separate sample of Z boson production generated with ALPGEN is used to cover the region 10 GeV $< m_{\ell\ell} <$ 40 GeV.

The *MLM* [9, 11] matching scheme of the ALPGEN generator is used to remove overlaps between the n and $n + 1$ parton samples.

For all but the diboson processes, separate samples are generated that include $b\bar{b}$ quark pair production at the matrix-element level. In addition, for the W+jets process, separate samples containing Wc+jets and $Wc\bar{c}$+jets events are produced.

The MC@NLO generator is used for the background of single-top s- and Wt-channel and AcerMC for t-channel production. The uncertainty due to the choice of $t\bar{t}$ generator is evaluated by comparing the predictions of MC@NLO with those of POWHEG [12] interfaced to HERWIG or PYTHIA.

The flavour labeling of jets in Monte Carlo simulation is done by spatially matching the jet with generator level partons: if a b-quark is found within $\Delta R = \sqrt{\Delta\eta^2 + \Delta\phi^2} < 0.3$ of the jet direction, the jet is labeled as a b-jet. If no b-quark is found the procedure is repeated for c-quarks and τ-leptons. A jet for which no such association could be made is labeled as a light-flavour jet. In this note, tau lepton induced jets are also treated as light jets.

2.2 Event selection

Events in the single lepton and dilepton $t\bar{t}$ channels are triggered using a high p_{T} single lepton trigger (electron or muon). The key objects for b-tagging are the reconstructed primary vertex, the calorimeter jets, and tracks reconstructed in the inner detector. Jets are reconstructed from topological clusters [13] of energy in the calorimeter using the anti-k_t algorithm with a distance parameter of 0.4 [14–16]. The jet energy is calibrated using p_{T}- and η-dependent correction factors [17]. The tracks are associated with the calorimeter jets with a spatial matching in $\Delta R(\mathrm{jet}, \mathrm{track}) = \sqrt{(\Delta\eta)^2 + (\Delta\phi)^2}$ [18]. Since a well-reconstructed primary vertex is important in b-tagging analyses, all measurements require at least three tracks associated with the primary vertex. The primary vertex is defined to be the vertex for which the associated tracks have the highest sum in squared transverse momenta. The $t\bar{t}$ analyses require isolated electrons and muons, as well as missing transverse momentum.

In all $t\bar{t}$ analyses, both in the single lepton and dilepton channels, the b-tagging efficiency measurement is performed in a sample comprising all lepton flavour combinations (e+jets and μ+jets or ee, $\mu\mu$ and $e\mu$).

2.2.1 Selection of the single lepton sample

In the single lepton channels (e+jets and μ+jets), the following event selection is applied:

- The appropriate single electron (with trigger thresholds at 20, 22 or 45 GeV, depending on the data taking period) or single muon trigger (trigger threshold at 18 GeV) has fired.
- The event contains exactly one reconstructed lepton with $p_{\mathrm{T}} > 25$ GeV (e) or $p_{\mathrm{T}} > 20$ GeV (μ), matching the corresponding high-level trigger object.
- In the e+jets channel, the missing transverse momentum $E_{\mathrm{T}}^{\mathrm{miss}} > 30$ GeV and the transverse mass $m_{\mathrm{T}}(l\nu) > 30$ GeV, while, in the μ+jets channel, $E_{\mathrm{T}}^{\mathrm{miss}} > 20$ GeV and $E_{\mathrm{T}}^{\mathrm{miss}} + m_{\mathrm{T}}(l\nu) > 60$ GeV. Here, $m_{\mathrm{T}}(l\nu)$ is the transverse mass of the selected lepton and the $E_{\mathrm{T}}^{\mathrm{miss}}$ vector. These cuts reduce the contribution from multijet background.
- The event is required to have at least four jets with $p_{\mathrm{T}} > 25$ GeV, $|\eta| < 2.5$ and a jet vertex fraction (JVF) with respect to the primary vertex of $|\mathrm{JVF}| > 0.75$. The JVF of a jet with respect to a vertex is defined as the ratio of the p_{T} of matched tracks originating from that vertex to the total p_{T} of all

tracks matched to the jet

$$\mathrm{JVF}(\mathrm{jet}_i, \mathrm{vtx}_j) = \frac{\sum_k p_{\mathrm{T}}(\mathrm{trk}_k^{\mathrm{jet}_i}, \mathrm{vtx}_j)}{\sum_n \sum_l p_{\mathrm{T}}(\mathrm{trk}_l^{\mathrm{jet}_i}, \mathrm{vtx}_n)} \tag{2}$$

and can be interpreted as the probability of the jet to originate from that vertex.

2.2.2 Background estimation in the single lepton channel

The dominant background in the single lepton channel arises from W boson production with associated jets (W+jets). Its estimate is based on the prediction from Monte Carlo simulation, corrected with scale factors derived directly from data. The correction of the overall normalisation is obtained with a *charge asymmetry* method [19]. The flavour composition of the W+jets sample is measured with a *tag counting* method [20], which provides scale factors for $Wb\bar{b}/c\bar{c}$+jets, Wc+jets and W with light flavour jets events used to correct Monte Carlo simulation predictions.

The second most important contribution to the background comes from multijet production and is measured directly in data using the *matrix method* which relies on finding a relationship between events with *real* and *fake* leptons which is described in [21]. Rate estimates of other backgrounds processes, such as single top, diboson and Z+jets production are obtained from Monte Carlo simulation.

Figure 1 shows the transverse mass $m_{\mathrm{T}}(l\nu)$ of the lepton and $E_{\mathrm{T}}^{\mathrm{miss}}$ vector, as well as $E_{\mathrm{T}}^{\mathrm{miss}}$ spectrum and in Figure 2 the jet multiplicity and jet p_{T} is presented. Those distributions are sensitive to a correct description of the multijet and W+jets backgrounds, and they all show a good agreement between the predicted background and signal contributions and data.

The final yields of the event selection for e+jets and μ+jets channels are presented in Table 1.

Source	e+jets			μ+jets		
$t\bar{t}$	17300	±	1700	28600	±	2800
W+jets	2800	±	400	5400	±	700
multijet	2300	±	1100	1800	±	400
single top	1430	±	110	2420	±	190
Z+jets	510	±	310	558	±	330
diboson	55.9	±	2.8	86	±	4
$\sum$	24500	±	2100	38900	±	2900
observed	21978			38188		

Table 1: The number of events passing the single lepton selection requirements corresponding to a luminosity of 4.7 fb^{-1} together with theoretical uncertainties on the cross sections ($t\bar{t}$, single top and Z+jets production) or uncertainties on the estimation directly from data (W+jets and multijet).

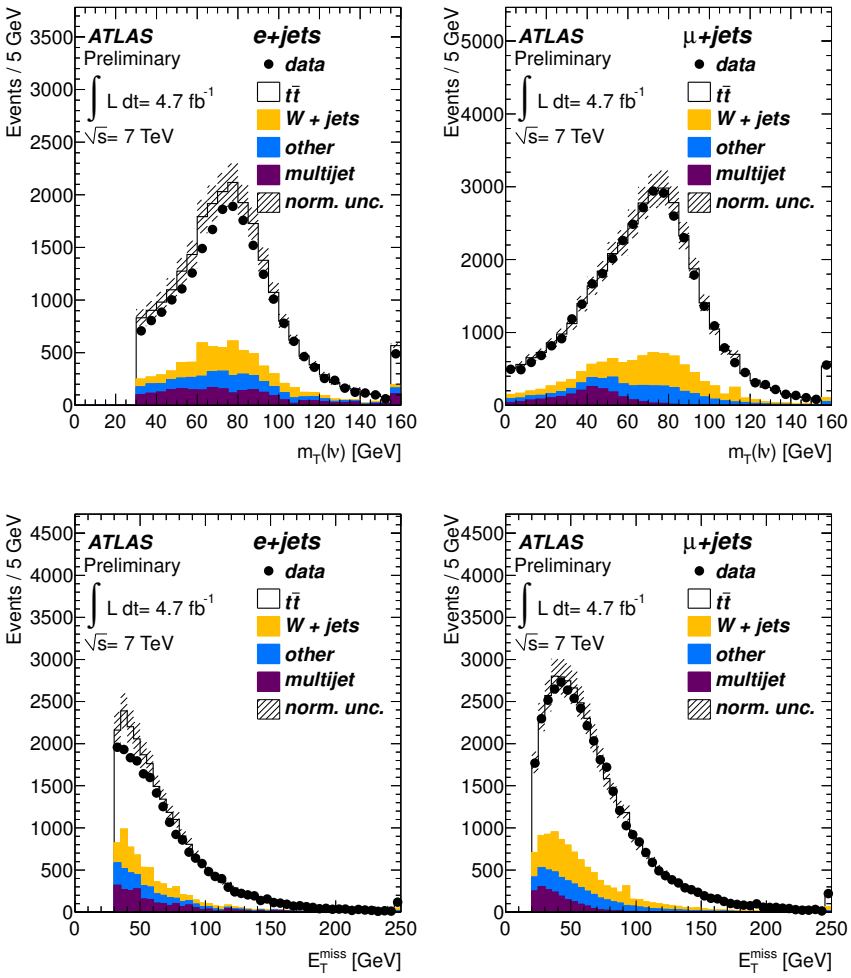

Figure 1: Transverse mass $m_{\mathrm{T}}(l\nu)$ of the lepton and $E_{\mathrm{T}}^{\mathrm{miss}}$ (upper row) for the e+jets channel (left) and μ+jets channel (right). $E_{\mathrm{T}}^{\mathrm{miss}}$ spectra (bottom row) for the e+jets channel (left) and μ+jets channel (right). All event selection criteria, including the requirement of at least 1 b-tagged jet, are applied. "Other" is a sum of contributions from Z+jets, single top and diboson production. The last bin is inclusive in all figures.

2.2.3 Selection of the dilepton sample

A very clean sample of $t\bar{t}$ events with dileptonic decays (ee, $\mu\mu$ and $e\mu$) can be obtained with the following event selection criteria:

- The appropriate single electron (trigger threshold at 20, 22 or 45 GeV depending on the data taking period) or single muon trigger (trigger threshold at 18 GeV) has fired.
- Exactly two oppositely charged leptons (ee, $\mu\mu$ or $e\mu$), with the electron candidate satisfying $p_{\mathrm{T}} > 25$ GeV, and the muon candidate $p_{\mathrm{T}} > 20$ GeV, where at least one of them must be associated with a high-level lepton trigger object.
- At least two jets with $p_{\mathrm{T}} > 25$ GeV, $|\eta| < 2.5$ and jet vertex fraction of $|\mathrm{JVF}| > 0.75$.

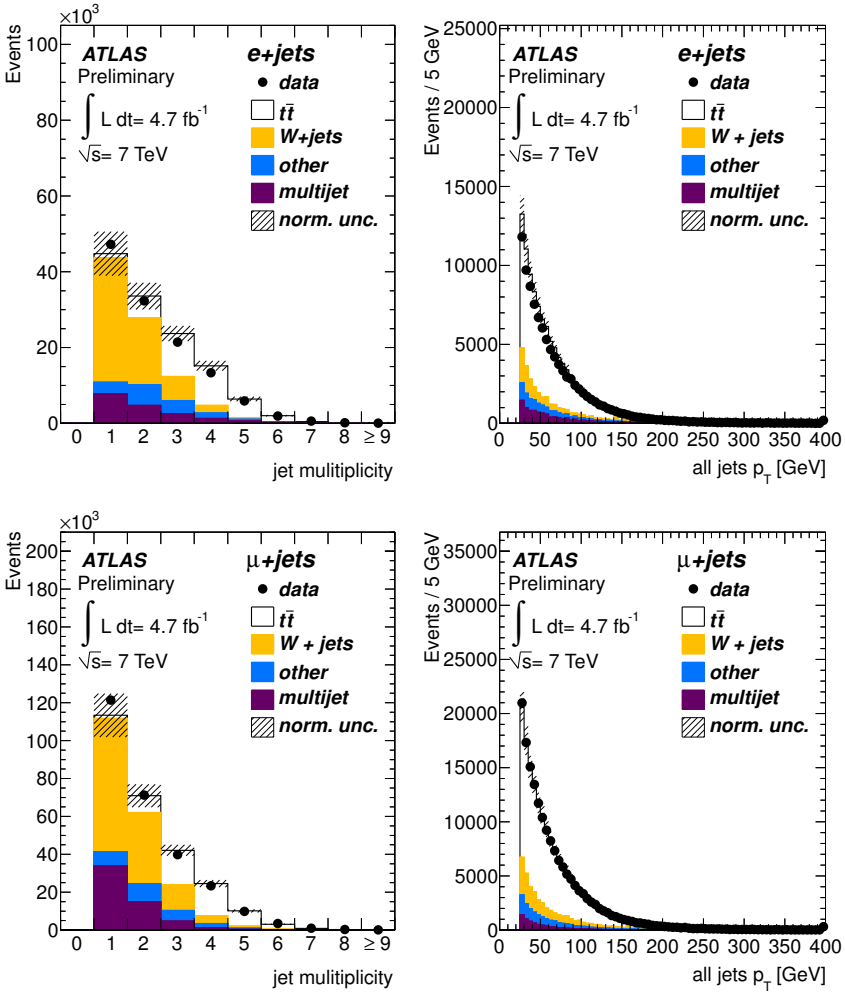

Figure 2: Jet multiplicity (left) in events passing the single lepton selection and the p_{T} of all jets (right) in the e+jets channel (upper row) and μ+jets channel (bottom row). "Other" is a sum of contributions from Z+jets, single top and diboson production. The last bin is inclusive in all figures.

- ee and $\mu\mu$ channels:
  - To suppress backgrounds from Z+jets and multijet events, the missing transverse momentum must satisfy $E_{\mathrm{T}}^{\mathrm{miss}} > 60$ GeV, and the invariant mass of the two leptons must differ by at least 10 GeV from the Z boson mass (Z mass veto): $|m_{\ell\ell} - m_Z| > 10$ GeV.
  - To suppress backgrounds from Υ and J/ψ decays, a low mass cut of $m_{\ell\ell} > 15$ GeV is applied.
- $e\mu$ channel:
  - In the $e\mu$ channel, no $E_{\mathrm{T}}^{\mathrm{miss}}$ or Z boson mass veto cuts are applied. However, the scalar sum of the transverse momenta of the jets and of the charged leptons $H_{\mathrm{T}}(\ell, \mathrm{jets})$, must satisfy $H_{\mathrm{T}} > 130$ GeV to further suppress background from the $Z(\rightarrow \tau\tau)$+jets production.

2.2.4 Background estimation in the dilepton channel

The dominant background in the dilepton channel is originating from fake leptons. This background contains W boson production with associated jets, single top in s- and t-channel, the single lepton decay of $t\bar{t}$

Source	N_{ee}	$N_{\mu\mu}$	$N_{e\mu}$
$t\bar{t}$	530 ± 50	1680 ± 170	4200 ± 400
$Z \to ee$ + jets	16 ± 6	–	–
$Z \to \mu\mu$ + jets	–	71 ± 28	–
$Z \to \tau\tau$ + jets	18 ± 7	70 ± 26	180 ± 70
diboson	8.4 ± 0.4	23.4 ± 1.2	67.2 ± 3.4
single top (Wt-channel)	26.8 ± 1.9	78 ± 6	204 ± 15
fake leptons	80 ± 40	43 ± 22	340 ± 170
$\sum$ MC + fake leptons	680 ± 60	1970 ± 180	5000 ± 400
observed	716	1970	5341

Table 2: The number of events passing the dilepton selection requirements presented for the corresponding $\ell\ell$-channel separately corresponding to a luminosity of 4.7 fb^{-1}. Shown uncertainties are the theoretical uncertainties on the cross section for simulation.

pairs and multijet events. There are two sources of faked prompt leptons: electron-like jets reconstructed as electrons or non-prompt leptons from a decay of a heavy flavour hadron within a jet.

In the dilepton sample the fake lepton background is estimated directly from data with a matrix method [21] for each of the three channels separately. All background processes which contain two prompt leptons (diboson, Z+jets and single top in the Wt-channel) are directly taken from the simulation.

The final yields for the three different channels are presented in Table 2, while the distributions, showing the leading jet p_{T} and η, invariant dilepton mass, $E_{\mathrm{T}}^{\mathrm{miss}}$ and H_{T}, can be found in Figures 3 and 4. In all figures a good agreement between data and simulation can be seen.

2.3 b-tagging algorithms

The b-tagging algorithms calibrated in this note are SV0, IP3D+SV1, JetFitterCombNN and MV1. More details about SV0 can be found in [22] while the IP3D+SV1 and JetFitterCombNN (also referred to as JetFitter+IP3D) algorithms are described in [23]. The MV1 algorithm is a neural network-based algorithm that uses the output weights of IP3D, SV1 and JetFitterCombNN as inputs.

The above b-tagging algorithms all provide an output weight w, discriminating between b-jets and non-b-jets. Lower values of w are assigned to c- and light-flavour jets, whereas the purity of b-jets increases with w. For each b-tagging algorithm a set of operating points, corresponding to a certain w cut value, are defined and calibrated:

- **SV0**: $\varepsilon_b^{\mathrm{sim}} = 50\%$
- **IP3D+SV1**: $\varepsilon_b^{\mathrm{sim}} = 60\%$, $\varepsilon_b^{\mathrm{sim}} = 70\%$, $\varepsilon_b^{\mathrm{sim}} = 80\%$
- **JetFitterCombNN**: $\varepsilon_b^{\mathrm{sim}} = 57\%$, $\varepsilon_b^{\mathrm{sim}} = 60\%$, $\varepsilon_b^{\mathrm{sim}} = 70\%$, $\varepsilon_b^{\mathrm{sim}} = 80\%$
- **MV1**: $\varepsilon_b^{\mathrm{sim}} = 60\%$, $\varepsilon_b^{\mathrm{sim}} = 70\%$, $\varepsilon_b^{\mathrm{sim}} = 75\%$, $\varepsilon_b^{\mathrm{sim}} = 85\%$

where $\varepsilon_b^{\mathrm{sim}}$ is the nominal b-tagging efficiency derived from an inclusive sample of simulated $t\bar{t}$ events.

3 b-tagging calibration methods

The methods presented in this note to measure the b-tagging efficiency exploit the large b-jet content of $t\bar{t}$ events. The *tag counting* method fits the multiplicity of b-tagged jets in $t\bar{t}$ candidate events while the *kinematic selection* method measures the b-tagging rate of the leading jets in the $t\bar{t}$ signal sample.

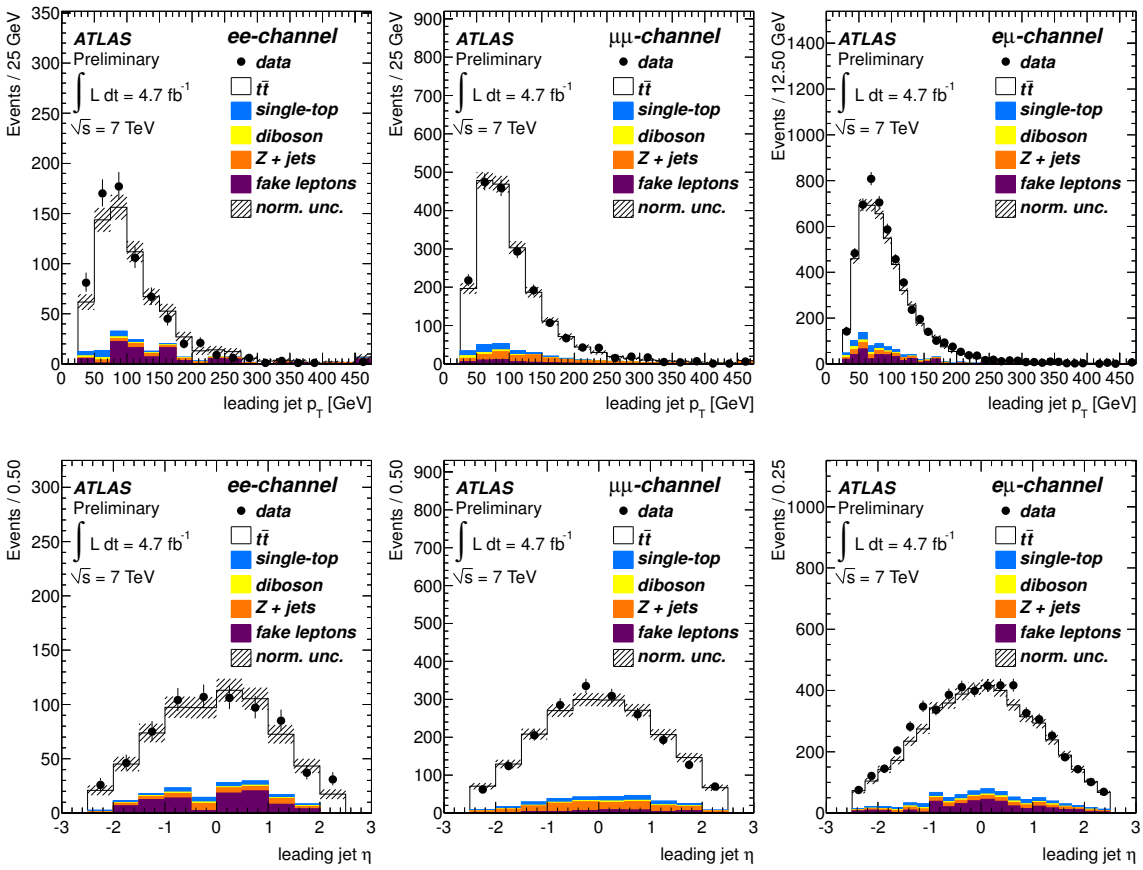

Figure 3: Distributions of the p_{T} (top) and η (bottom) of the leading jet for the ee, $\mu\mu$ and $e\mu$ channels.

Finally, the *kinematic fit* method uses a fit of the $t\bar{t}$ event topology to extract highly purified sample of b-jets from which the b-tagging efficiency is obtained.

The tag counting and kinematic selection methods can be applied to both the single lepton and dilepton decay channels, whereas the kinematic fit method is restricted by construction to the single lepton channel.

3.1 Tag counting method

The tag counting method makes use of the fact that since the branching fraction of $t \to Wb$ in the Standard Model is very close to unity, each $t\bar{t}$ event is expected to contain exactly two real b-jets. If there were no other sources of b-jets and if only b-jets were b-tagged, the expected number of events with two b-tagged jets would be $\varepsilon_b^2 N_{\mathrm{sig}}$ while the number of events with one b-tagged jet would be $\varepsilon_b\,(1-\varepsilon_b)\,2N_{\mathrm{sig}}$, where N_{sig} is the number of $t\bar{t}$ signal events.

In reality, the mean number of reconstructed (or tagged) b-jets in a $t\bar{t}$ event is not exactly two, since the b-jets from the top quark decays can be out of the detector acceptance, and additional b-jets can be produced through gluon splitting. Moreover, c-jets and light flavour jets, which come from the hadronic W boson decay or initial or final state radiation, can be tagged as b-jets and consequently contribute to the number of b-tagged jets in the event. These effects are taken into account by evaluating the expected fractions, F_{ijk}, of events containing i b-jets, j c-jets and k light-flavour reconstructed jets that pass the event selection. The F_{ijk} fractions are estimated from Monte Carlo simulation and are derived separately

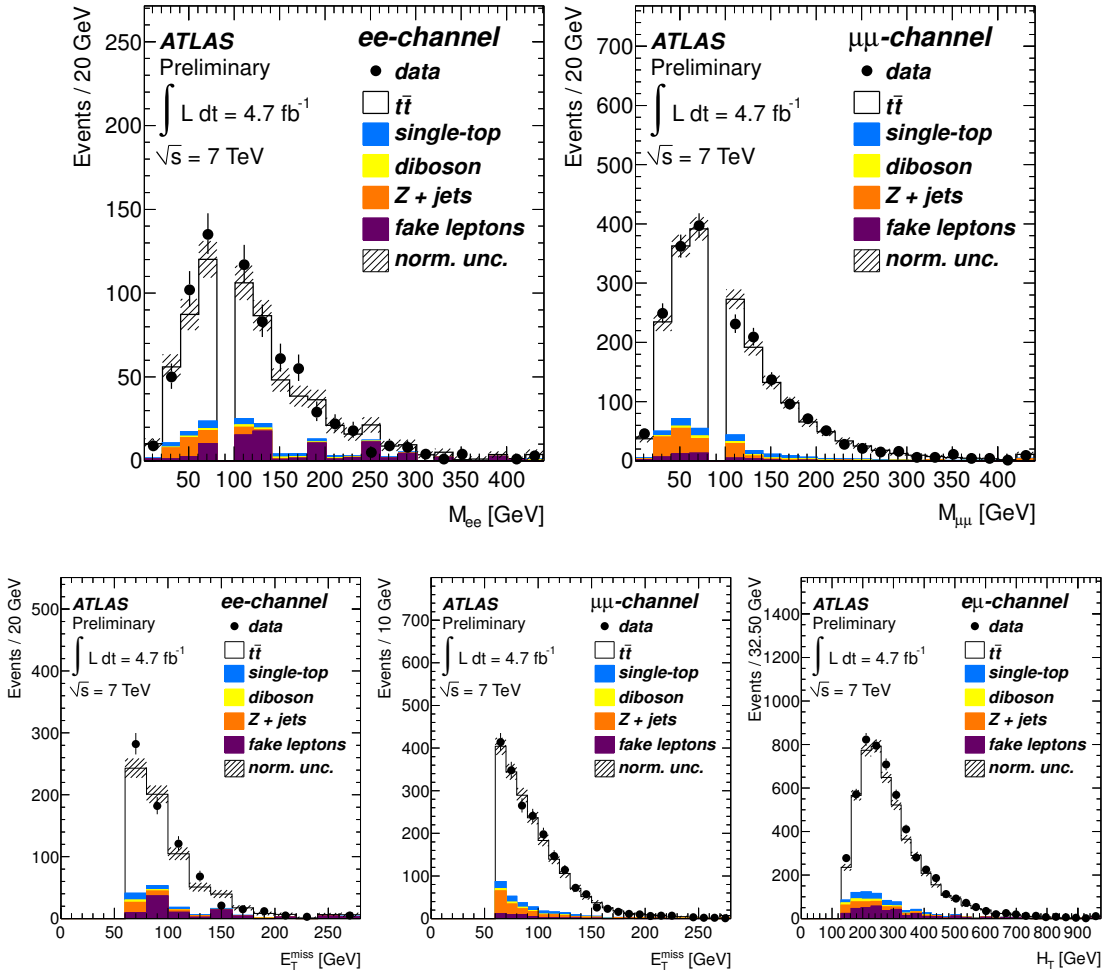

Figure 4: Distributions of the invariant mass of two leptons in the ee- and $\mu\mu$-channels (top) and the missing transverse momentum in the ee- and $\mu\mu$-channels and H_{T} in the $e\mu$-channel (bottom).

for the $t\bar{t}$ signal and the various background processes. The expected number of events with n b-jets is calculated as the sum of all these contributions. The b-tagging efficiency can be extracted by fitting the expected event counts to the observed counts.

The expected number of $t\bar{t}$ signal events with n b-tagged jets, $< N_n >$, is calculated as

$$< N_n > = \sum_{i,j,k} \Big\{ (\sigma_{t\bar{t}} \cdot \mathrm{BF} \cdot A_{t\bar{t}} \cdot \mathcal{L} \cdot F_{ijk}^{t\bar{t}} + N_{\mathrm{bkg}} \cdot F_{ijk}^{\mathrm{bkg}}) \times \sum_{i'+j'+k'=n} \binom{i}{i'} \cdot \varepsilon_b{}^{i'} \cdot (1-\varepsilon_b)^{i-i'} \cdot \binom{j}{j'} \cdot \varepsilon_c{}^{j'} \cdot (1-\varepsilon_c)^{j-j'} \cdot \binom{k}{k'} \cdot \varepsilon_l{}^{k'} \cdot (1-\varepsilon_l)^{k-k'} \Big\}, \quad (3)$$

where i, j and k (i', j' and k') represent the number of pretagged (tagged) b-, c- and light-flavour jets. BF is the branching fraction to each final state, (e+jets, μ+jets, ee, $\mu\mu$ and $e\mu$), including leptonically decaying τ-leptons, $A_{t\bar{t}}$ is the event selection efficiency for that particular final state and $\mathcal{L}$ is the integrated luminosity. The binomial coefficients account for the number of arrangements in which the n-tags can be distributed. The efficiencies to mis-tag a c-jet or light-flavour jet as a b-jet, ε_c and ε_l respectively, are fixed to the values found in Monte Carlo simulation but with data driven scale factors applied [24]. N_{bkg}

is the number of background events. In the dilepton channel, the expected number of Z+jets background events, $N_{Z+\text{jets}}$, is treated separately from other backgrounds sources, N_{other}, since it gives the largest contribution of all simulated background processes.

To apply the method as a function of p_{T}, the F_{ijk} fractions are computed in p_{T} bins using only the jets in each event that fall in a given p_{T} bin. For both signal and background the dominant fraction is F_{000} which occurs when no jets fall in that particular p_{T} bin. Since a single event can contribute to several p_{T} bins, this method maximises the use of the available jets in the sample.

The dominant $t\bar{t}$ F_{ijk} contributions in the single lepton channel are shown in Table 3 for all jets with p_{T} above 25 GeV and Table 4 for the 30 – 40 GeV p_{T} bin. The corresponding F_{ijk} fractions in the dilepton channel are shown in Table 5.

F_{ijk}	$t\bar{t}$ e channel	F_{ijk}	e channel backgrounds	F_{ijk}	$t\bar{t}$ μ channel	F_{ijk}	μ channel backgrounds
F_{202}	29.1±0.1%	F_{004}	51.0±0.5%	F_{202}	28.9±0.1%	F_{004}	53.0±0.4%
F_{211}	14.8±0.1%	F_{013}	13.6±0.2%	F_{211}	15.1±0.1%	F_{013}	13.8±0.1%
F_{203}	12.9±0.1%	F_{005}	12.0±0.2%	F_{203}	12.9±0.1%	F_{005}	10.8±0.2%
F_{103}	9.3±0.1%	F_{103}	3.8±0.1%	F_{103}	9.2±0.1%	F_{103}	4.0±0.1%
F_{212}	8.3±0.1%	F_{014}	3.4±0.1%	F_{212}	8.4±0.1%	F_{022}	3.4±0.1%

Table 3: The leading F_{ijk} fractions for jets with $p_{\text{T}} > 25$ GeV in the e+jets and μ+jets channels, obtained from the simulated $t\bar{t}$ and inclusive background samples. Uncertainties are statistical only.

F_{ijk}	$t\bar{t}$ e channel	F_{ijk}	e channel backgrounds	F_{ijk}	$t\bar{t}$ μ channel	F_{ijk}	μ channel backgrounds
F_{000}	41.0±0.1%	F_{001}	37.6±1.5%	F_{000}	40.7±0.1%	F_{001}	37.4±0.5%
F_{001}	25.1±0.1%	F_{000}	37.4±0.8%	F_{001}	25.3±0.1%	F_{000}	36.4±0.3%
F_{100}	11.6±0.1%	F_{002}	13.8±0.5%	F_{100}	11.4±0.1%	F_{002}	14.4±0.2%
F_{101}	6.5±0.1%	F_{003}	2.7±0.3%	F_{101}	6.5±0.1%	F_{003}	2.8±0.1%
F_{010}	5.3±0.1%	F_{100}	2.4±0.1%	F_{002}	5.3±0.1%	F_{010}	2.5±0.1%

Table 4: The leading F_{ijk} fractions for jets with p_{T} between 30 and 40 GeV in the e+jets and μ+jets channels, obtained from the simulated $t\bar{t}$ and inclusive background samples. Uncertainties are statistical only.

Different approaches are considered in the single lepton and dilepton analyses to take into account the contributions from background events. In the single lepton channel, the 0-jet bin is dominated by multijet and W+jets backgrounds and is therefore not included in the fit. The multijet background is subtracted from the n-tag distribution prior to performing the fit since the F_{ijk} fractions cannot be reliably estimated from Monte Carlo simulation. For the remaining background processes, dominated by W+jets, F_{ijk}^{bkg} values are calculated from Monte Carlo simulations and included in the fit to extract the b-tagging efficiency. In the dilepton channel the main background obtained from Monte Carlo simulation, Z+jets, is included into the F_{ijk}^{bkg} parameters along with much smaller contributions from single top and diboson production. The dilepton channel suffers from a lower branching ratio but has a higher purity than the single lepton channel so the 0-tag bin is kept to minimize the statistical uncertainty of the measurement.

The extraction of parameters in Equation 3 from the data is performed using a likelihood fit with the `MINUIT` program. The likelihood function used is

$$L = \text{Gaus}(\sigma_{t\bar{t}}|\sigma_{t\bar{t},MC}, \delta_{\sigma_{t\bar{t},rmMC}})\ \text{Gaus}(\tilde{N_{\text{bkg}}}|N_{\text{bkg,MC}}, \delta_{N_{\text{bkg}}}) \prod_{n-tags} \text{Pois}(N_n| < N_n >). \quad (4)$$

ee channel					
F_{ijk}	$t\bar{t}$	F_{ijk}	Z+jets	F_{ijk}	Other bkgs
F_{200}	37.6±0.6%	F_{002}	46.0±4.2%	F_{101}	34.9±4.2%
F_{201}	21.7±0.5%	F_{003}	26.6±3.3%	F_{002}	20.3±1.5%
F_{101}	16.6±0.4%	F_{004}	6.6±1.5%	F_{200}	11.5±1.4%
F_{202}	7.5±0.3%	F_{011}	4.5±1.3%	F_{201}	10.5±1.4%
F_{102}	5.9±0.2%	F_{012}	4.0±1.2%	F_{102}	8.2±1.6%
$\mu\mu$ channel					
F_{ijk}	$t\bar{t}$	F_{ijk}	Z+jets	F_{ijk}	Other bkgs
F_{200}	37.8±0.3%	F_{002}	47.2±3.2%	F_{101}	31.9±1.5%
F_{201}	21.6±0.3%	F_{003}	20.4±1.1%	F_{002}	21.0±1.2%
F_{101}	16.1±0.2%	F_{004}	8.6±1.3%	F_{200}	11.6±1.5%
F_{202}	8.3±0.2%	F_{011}	4.6±1.0%	F_{201}	10.8±1.4%
F_{102}	6.2±0.1%	F_{012}	3.5±1.0%	F_{102}	6.7±1.2%
$e\mu$ channel					
F_{ijk}	$t\bar{t}$	F_{ijk}	Z+jets	F_{ijk}	Other bkgs
F_{200}	39.8±0.2%	F_{002}	56.2±1.7%	F_{101}	33.3±1.5%
F_{201}	23.1±0.2%	F_{003}	19.7±1.4%	F_{002}	21.2±0.9%
F_{101}	15.7±0.1%	F_{004}	4.9±0.7%	F_{200}	15.1±1.0%
F_{202}	7.4±0.1%	F_{011}	5.7±1.0%	F_{201}	7.3±0.8%
F_{102}	5.7±0.1%	F_{012}	1.7±0.6%	F_{102}	8.5±0.8%

Table 5: The leading F_{ijk} fractions in the ee, $\mu\mu$ and $e\mu$ channels, obtained from the simulated $t\bar{t}$, Z+jets and other background samples. Only the statistical uncertainty is shown.

The number of events in each n-tag bin is described by a Poisson probability with an average value corresponding to the number of expected events. The $t\bar{t}$ cross section and N_{bkg} are floating parameters of the fit but are each constrained by a Gaussian distribution with a width of one standard deviation of the respective theory uncertainties. The uncertainty introduced by the Monte Carlo simulation statistics has been estimated from the uncertainties given in the F_{ijk} tables (Tables 3, 4 and 5) and is found to be negligible.

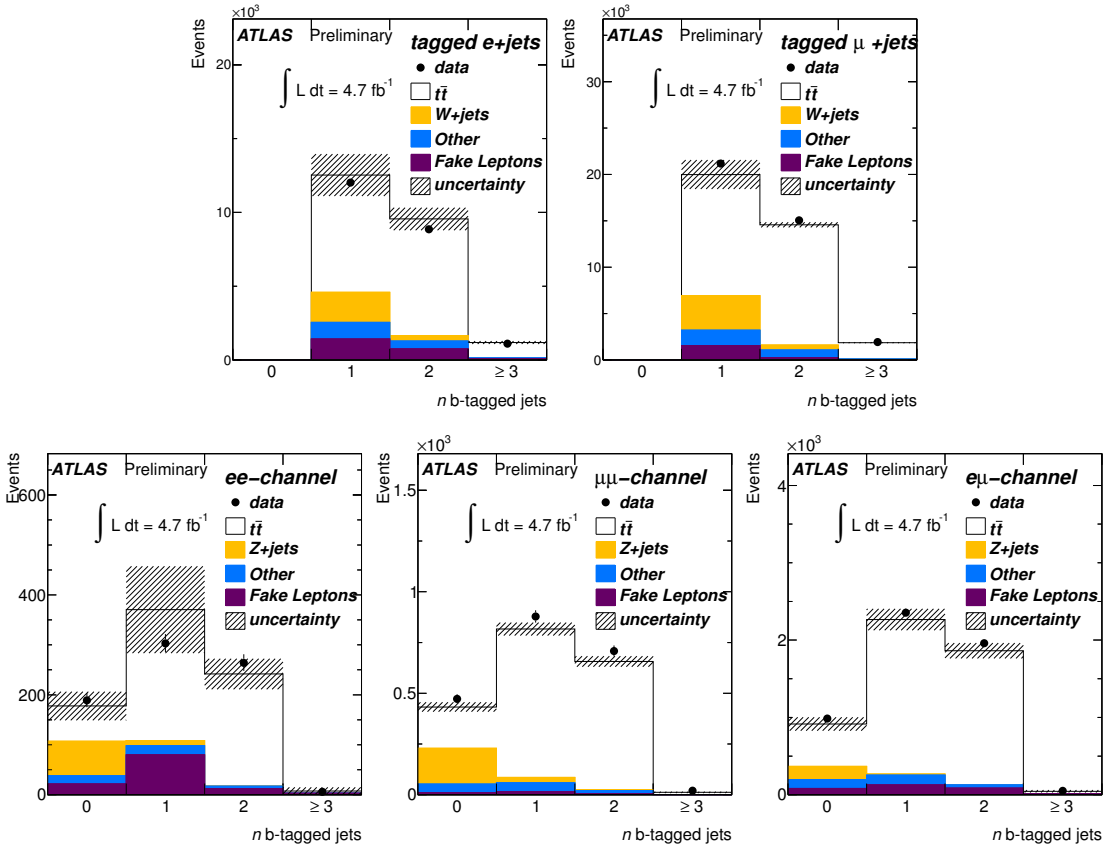

Figure 5: The b-tagged jet multiplicity distribution in Monte Carlo simulation superimposed with the distribution observed in data for e+jets (top left), μ+jets (top right), ee (bottom left), $\mu\mu$ (bottom middle) and $e\mu$ (bottom left) channels.

In Figure 5 the number of fitted b-tagged jets for all of the channels in comparison to Monte Carlo simulation are shown. The measured b-tagged jet multiplicity distributions are well reproduced by the Monte Carlo simulation.

3.2 Kinematic selection method

The kinematic selection method relies on the knowledge of the flavour composition of the $t\bar{t}$ signal and background samples, and extracts the b-tagging efficiency by measuring the fraction of b-tagged jets in data. Given an expected fraction of b-, c- and light-flavour jets, as well as the c- and light-flavour jet mis-tag efficiencies, the fraction of b-tagged jets in data is given by

$$f_{b\text{–tag}} = \varepsilon_b f_{b\text{–jets}} + \varepsilon_c f_{c\text{–jets}} + \varepsilon_l f_{l\text{–jets}} + \varepsilon_{\text{fake}} f_{\text{fake}} \tag{5}$$

which can be rearranged in the following way to solve for the b-tagging efficiency, ε_b:

$$\varepsilon_b = \frac{1}{f_{b-\text{jets}}} \cdot \left(f_{b-\text{tag}} - \varepsilon_c f_{c-\text{jets}} - \varepsilon_l f_{l-\text{jets}} - \varepsilon_{\text{fake}} f_{\text{fake}} \right). \tag{6}$$

Here, $f_{b-\text{jets}}$, $f_{c-\text{jets}}$ and $f_{l-\text{jets}}$ are the expected fractions of b-, c- and light-flavour jets from simulated events and the ε_c and ε_l are the mis-tag efficiencies for c- and light-flavour jets to be tagged as b-jets, which are taken from Monte Carlo simulation and corrected for data-to-simulation scale factors from [25, 26]. They are obtained from the sum of simulated events from all processes, assuming the expected jet kinematics and the expected signal and background contributions to the analysed sample. f_{fake} is the fraction of jets from the fake lepton (in the dilepton channel) or multijet (in the single lepton channel) background and is determined from data. The flavour fractions are calculated with respect to the sum of jets from Monte Carlo simulation and follow the relation $f_{b-\text{jets}} + f_{c-\text{jets}} + f_{l-\text{jets}} + f_{\text{fake}} = 1$. The flavour composition of the jet sample obtained after applying a dilepton selection is shown in Figure 6 binned in both p_{T} and η. The expected fraction of b-tagged fake lepton or multijet events, $\varepsilon_{\text{fake}}$, is estimated from data, as detailed below.

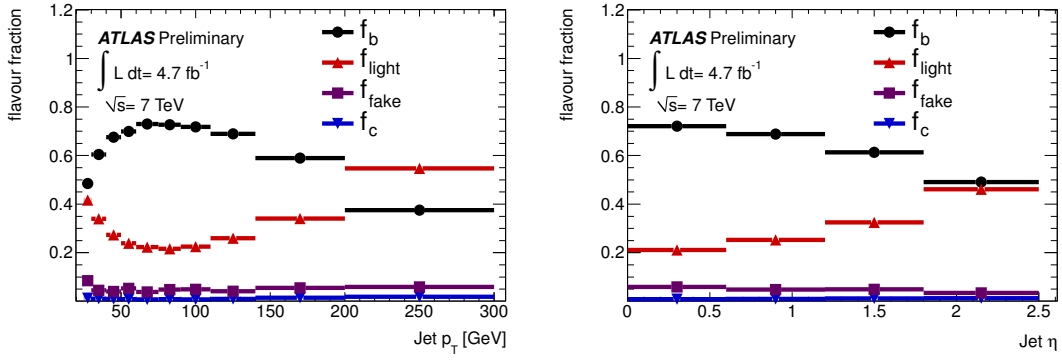

Figure 6: Expected jet flavour composition of the two leading jets in the selected dilepton events as a function of jet p_{T} (left) and η (right).

The fraction of b-tagged multijet events in the single lepton channel, $\varepsilon_{\text{fake}}$, is measured in a data control region enriched in multijet events. The control region is obtained by reverting the $E_{\text{T}}^{\text{miss}}$ and $m_{\text{T}}(l\nu)$ selection criteria:

- e+jets channel: 5 GeV $< E_{\text{T}}^{\text{miss}} <$ 30 GeV and $m_{\text{T}}(l\nu) <$ 25 GeV;
- μ+jets channel: 5 GeV $< E_{\text{T}}^{\text{miss}} <$ 15 GeV or $E_{\text{T}}^{\text{miss}} + m_{\text{T}}(l\nu) <$ 60 GeV.

Moreover, the leptons in the control region are only required to fulfill looser selection criteria (so called loose leptons). Loose muons are not required to fulfill any isolation criteria, while the isolation for loose electrons is less strict than for the *tight* criterion used in the baseline event selection [27]. From the events measured in the control region in data the predicted contributions of the $t\bar{t}$, single top, diboson, W+jets and Z+jets processes obtained from Monte Carlo simulation are subtracted.

In the dilepton channel, the fraction of b-tagged jets coming from the fake lepton background $\varepsilon_{\text{fake}}$ is determined by taking into account only those events in which the charge of both leptons have the same sign. The remaining event selection criteria are required to be passed. Since it is expected that neither the dileptonic $t\bar{t}$ decay nor the background processes Z+jets or single top can produce same sign events, a sample which is very enriched in events having at least one fake lepton is obtained.

To increase the signal-to-background ratio as well as the purity of the analysed sample, the events in the single lepton channel are required to, in addition to the selection from Section 2.2.1, have at least one

jet b-tagged with the MV1 tagging algorithm at an operating point corresponding to an efficiency of 70%. Based on which jet is b-tagged, the single lepton sample is split in two sub-samples in the following way:

- If the leading jet is b-tagged, the b-tagging rate of the next three jets is measured (L234 sample).
- If the next-to-leading jet is b-tagged, the b-tagging rate of the leading jet is measured (L1 sample).

Subsequently, jets are divided in bins of p_{T}, in which the number of b-tagged jets from each selection is counted. To calculate the b-tagging efficiency, the combined L1+L234 sample is used.

In the dilepton analysis, the b-jet fraction of the sample is increased by using only the two leading jets in each event, as this reduces the contamination of c- and light-flavour jets originating from gluon radiation.

3.3 Kinematic fit based method

The kinematic fit method is based on the selection of a high purity b-jet sample by applying a kinematic fit [28–30] to the events passing the selections described in Section 2.3. The kinematic fit performed on the single lepton $t\bar{t}$ event topology provides a mapping between the reconstructed jets and the lepton onto the b-jets originating directly from the top quark decays and the jets (leptons) from the subsequent hadronic (leptonic) W-boson decay. The kinematic fit exploits the masses of the two top quarks and W bosons as constraints, leading to four constraints in total with one unmeasured parameter resulting in three degrees of freedom. The fit, which is based on a χ^2-minimisation method, is performed on all permutations the six highest p_{T} jets, and the permutation with the lowest value in χ^2 is retained.

The b-tag efficiency is measured with the jets assigned by the fit to be the b-jet on the leptonic side of the event. While the kinematic fit selects the correct jet association with a reasonably high efficiency ($\approx 60\%$), the permutation with the lowest χ^2 is not always the correct one. In addition to the combinatorial background the sample still contains physics background, such as single top and W+jets events. Therefore, a high purity weight distribution of b-jets can only be obtained from data by using a statistical background subtraction. This subtraction is done by dividing the sample into two orthogonal sub-samples based on information about the jets associated to the hadronic side of the event: the first sub-sample ("signal sample") results from applying additional cuts resulting in a higher fraction of correct mappings, while the second sub-sample ("background sample") is enriched in incorrect mappings. The additional cuts applied to the signal sample are:

- The jet identified by kinematic fitting with the b-jet on the hadronic side of the event needs to be b-tagged by the MV1 tagging algorithm at the 70% efficiency operating point. This is applied to suppress the W+jets events and incorrect permutations.
- The jets associated with the hadronic W-decay must not be b-tagged by the MV1 b-tagging algorithm at the 70% efficiency operating point.
- Only events with six or less jets with $p_{\mathrm{T}} > 25$ GeV are considered.

The background sample is instead defined by removing the b-tagging requirement on the hadronic b-jet and the jet multiplicity requirement and inverting the b-tagging veto on the jets associated to the W decay:

- One of the jets assigned by the kinematic fit to the hadronic W decay is required to be b-tagged by the MV1 tagging algorithm at the 70% efficiency operating point.

To verify that the signal sample is enriched in correct mappings at low values of fit χ^2, while the background sample is dominated by incorrect mappings at all values of fit χ^2, a truth-match based on

a ΔR cut to the original partons of the hard interactions is performed in Monte Carlo simulation. Here, groupings of partons, hadron-level jets and reconstructed jets are chosen in a way that minimise the sum of their respective distances in the $\eta - \phi$ plane. Such a triplet is considered to be matched if the respective sum of the three distances in the $\eta - \phi$-plane passes the requirement $(\Delta R_{\text{parton}} + \Delta R_{\text{jet}}^{\text{hadron}} + \Delta R_{\text{jet}}^{\text{reco}}) < 0.5$. Due to e.g. unreconstructed jets, it will not always be possible to define the above triplets, and thus a portion of events will remain unmatched. The unmatched mappings remain in the analysis as they are, in Monte Carlo simulations the truth b-jets are taken into account independent from there matching status.

The χ^2 distribution of both the signal and background samples are shown together with the result of the truth-match in Figure 7. As desired, the signal sample has a sizable fraction of correct mappings, while the background sample almost exclusively is made up of unmatched or incorrect mappings. Furthermore, the correct mappings have predominantly a low χ^2-value, while the high χ^2-region is fully dominated by incorrect and unmatched mappings.

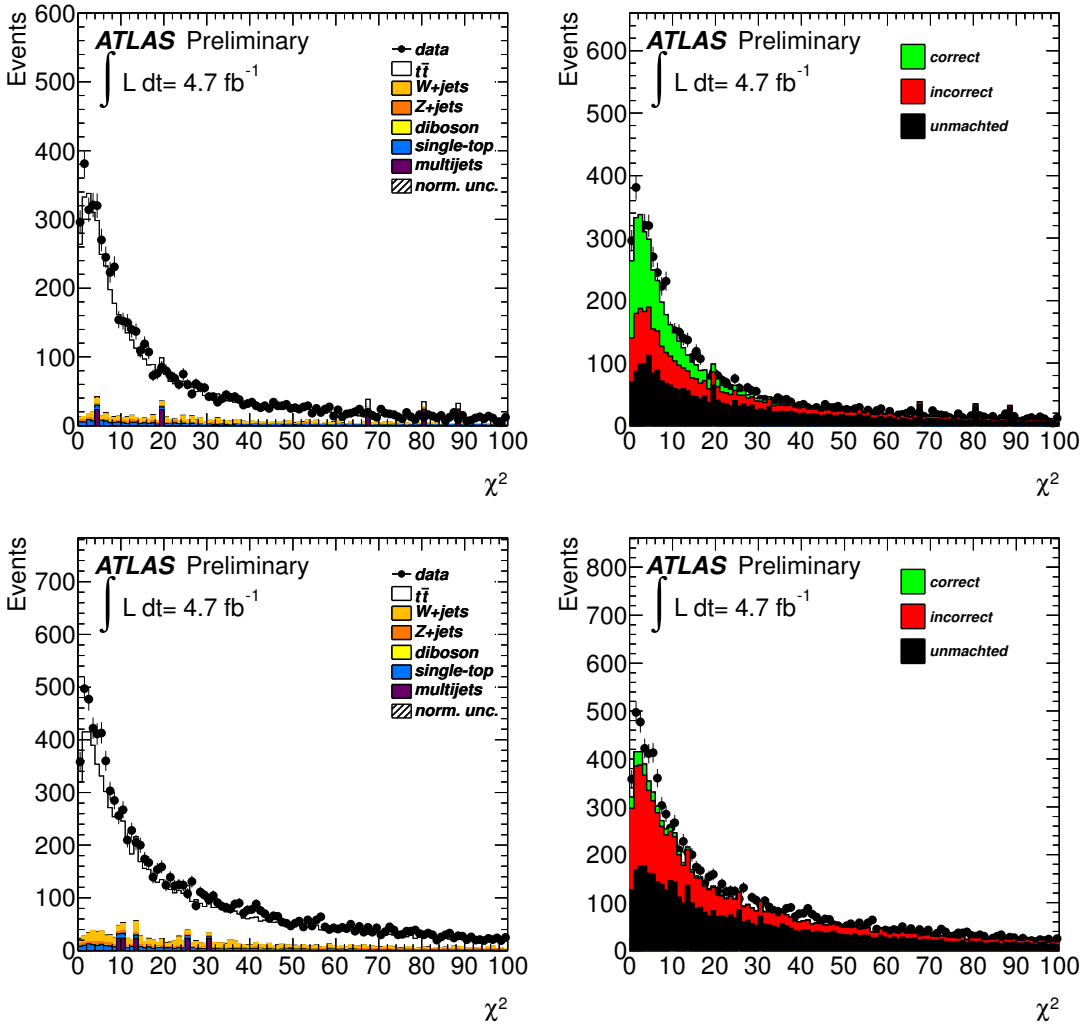

Figure 7: The χ^2 distributions of events in the signal sample (upper row) and the background sample (lower row). The overlaid truth-match is shown in the plots on the right.

The remaining background of incorrect mappings in the signal sample selected from data can therefore be estimated from the background sample. As events with high values of χ^2 are predominantly incorrect mappings in both sub-samples, the background sample prediction can be normalised at high χ^2

values ($\chi^2 > 25$), by using the scale factor

$$S_{\mathrm{BG}} = \frac{\int_{25}^{\infty} d\chi_S^2}{\int_{25}^{\infty} d\chi_B^2}. \tag{7}$$

The background-subtracted b-tag weight distribution of the b-jet from the leptonic decay in the signal sample, from which the b-tagging efficiency is eventually extracted, is subsequently derived by subtracting the b-tag weight distribution in the background sample, scaled according to Equation 7. As this subtraction scheme is performed on data, one significant advantage of this method is the reduced dependence on Monte Carlo simulation.

For the background subtraction method to work correctly it is imperative that the shape of the χ^2 distribution of the non-b portion of the background sample agrees with that of the non-b portion of the signal sample. This is verified in the upper left plot of Figure 9. It is furthermore crucial that the shapes of the b-tag weight distribution for b-jets and non-b-jets have the same shape in the signal and background samples. This is shown to be the case for the JetFitterCombNN b-tagging algorithm in Figure 8 and holds true for all b-tagging algorithms.

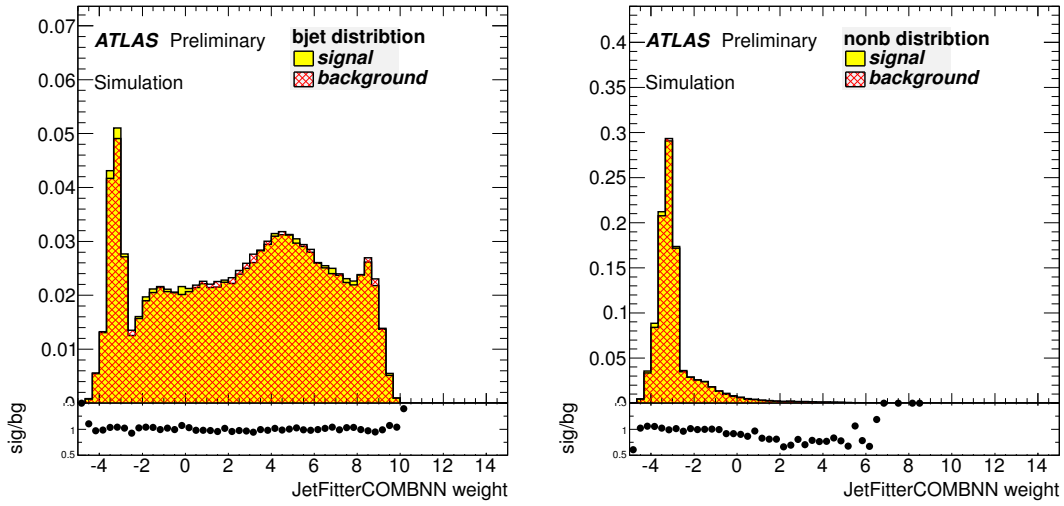

Figure 8: The weight distribution for the JetFitterCombNN b-tagging algorithm for b-jets (left) and non-b-jets (right) in the signal and background samples. The signal and background shapes are found to agree.

The measurement of the b-tagging efficiency is based on the b-tag weight distribution (see Section 2.3) of the sample of b-jets on the leptonic side of the event. An important advantage of this method is that a continuous calibration of the b-tag weight distribution is feasible, as the full distribution is reconstructed. The b-tag efficiency for a given operating point, corresponding to a certain weight cut w_{cut}, can be calculated using the (normalised to unity) weight distribution $T(w)$ of the selected b-jet sample after the background subtraction by integration above the threshold w_{cut}:

$$\varepsilon(w_{\mathrm{cut}}) = \int_{w_{\mathrm{cut}}}^{\infty} T(w)\,\mathrm{d}w. \tag{8}$$

Depending on the available statistics the measurement of the b-tag efficiency can be binned in any parameter, for example p_{T} or η.

The complete sequence of calibration steps for the MV1 b-tagging algorithm in the inclusive bin (25 GeV $< p_{\mathrm{T}} <$ 200 GeV) is presented in Figure 9. After a correct scaling of the background sample

(upper row) the prescription results in a background-subtracted distribution of the MV1 weight (lower left plot). Using Equation 8 the efficiency is derived (lower right). It is shown that the method applied to simulated events ("expected") describes the distribution obtained from the sample of true b-jets in Monte Carlo simulated events. The scaling factor quoted is the ratio of the efficiency measured in data and the efficiency calculated from true b-jets in simulated events.

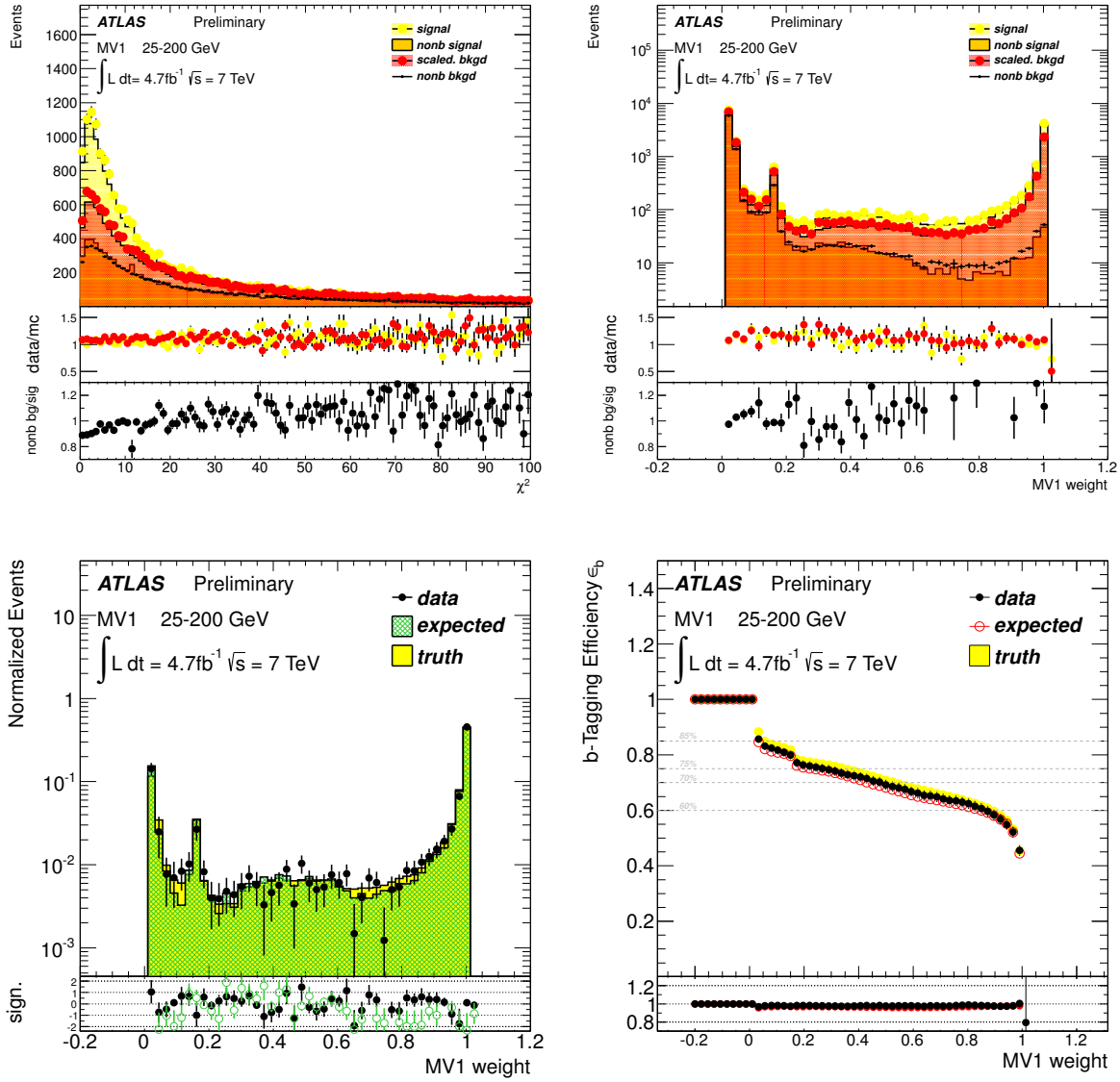

Figure 9: The χ^2 and MV1 weight distributions in the signal and scaled background samples with the respective non-b contributions outlined (upper row), background-subtracted MV1 weight distribution and the efficiency of the MV1 b-tagging algorithm (lower row). The expected distributions are obtained by performing the kinematic fit method on simulated events while the truth distributions correspond to those for simulated b-jets. Note that the MV1 weight distribution is shown with a logarithmic scale.

4 b-Tagging calibration results

In this section, the results for all $t\bar{t}$ based b-tagging efficiency measurements are given. The uncertainty of the scale factors, defined in Equation 1, include both the statistical uncertainty from the data and systematic uncertainties. The systematic uncertainties are affecting both the numerator and the denominator of Equation 1.

4.1 Systematic uncertainties

The estimates of systematic uncertainties in the $t\bar{t}$ analyses follow closely those used in the $t\bar{t}$ cross section analyses [24].

Mis-tagging efficiencies

In both the tag counting and the kinematic selection methods, the mis-tagging efficiencies for c- and light-flavour jets, ϵ_c and ϵ_l, directly enter the expression used to obtain the b-tagging efficiency. The efficiencies in simulated events are adjusted by the data-to-simulation scale factors [25, 26] and the efficiencies are then varied within the uncertainties of these correction factors, which range from approximately 12% to 50%.

$t\bar{t}$ cross section

In the kinematic selection method, the $t\bar{t}$ cross section is used to normalise the expected $t\bar{t}$ signal relative to the backgrounds. The $t\bar{t}$ cross section is varied by 10% [31].

Background normalisation

In all analyses the dominant backgrounds are estimated using data driven techniques. In the single lepton final state, the dominant background comes from W+jets production, and the normalisation of this background is varied by 13% based on the consideration of the various scale factors to correct the Monte Carlo expectations. In the dilepton final states the Z+jets normalisation uncertainty depends on the number of jets in the final state. An inclusive normalization uncertainty of 4% is assumed and an additional term of 24% per jet is added in quadrature. In the single lepton analyses, where the Z+jets background is substantially smaller, it is normalised to the theoretical cross section and varied by 60% [21].

The multijet background in the kinematic selection measurement is varied by 50% in the e+jets, which is a very conservative assumption, and covers any differences in kinematic distributions arising from mismodelling of the multijet background. In the μ+jets channel by comparing estimates based on two different control regions, the uncertainty on the multijet sample normalisation can be reduced to 20%. The tag counting single lepton measurement estimates this systematic uncertainty by migrating multijet events to and from the b-tagged sample. The fake lepton background in the tag counting and kinematic selection dilepton analysis is varied by 50%.

The single top and diboson backgrounds are normalised to their theoretical cross sections. The single top Wt-channel is varied by 8% [32], the t- and s-channels by 4% [33, 34] and the diboson sample by 5% [35].

Background flavour composition

The flavour composition of all background samples except W+jets is taken from simulation and not assigned a systematic uncertainty. For the W+jets background the scale factors for heavy flavour (HF)

events ($W\bar{b}$+jets, $Wc\bar{c}$+jets and Wc+jets) are varied within their uncertainties. Sources of systematic uncertainty that effect the HF scale factors in W+jets events often also affect the calibration methods described in this note directly. Examples of such systematic uncertainties are the uncertainties on the $t\bar{t}$ cross section and W+jets normalization. To account for such correlations, these uncertainties are evaluated by coherently evaluating their impact on all components of the analysis.

In the kinematic selection methods the b-tagging efficiency ε_{fake} for jets from the multijet background in the single lepton analysis and the fake lepton background in the dilepton analysis is measured in a control region in data. In the dilepton analysis an uncertainty of 50% is assumed, while in the single lepton analysis the uncertainty is obtained by comparing baseline result with the b-tagging efficiencies measured in events from the *jet electron model* [36].

Jet reconstruction efficiency, energy scale and resolution

The systematic uncertainty originating from the jet energy scale (JES) [17] is obtained by scaling the p_{T} of each jet in the simulation up and down by the estimated uncertainty on the jet energy scale. The nominal jet energy resolution (JER) in Monte Carlo simulation and data are found to be compatible, but a systematic uncertainty is assigned to cover the effect of possible residual differences by smearing the jet energy in simulated events. The full difference from the nominal result is taken as the uncertainty. The jet reconstruction efficiency (JRE) was derived using a tag-and-probe method in dijet events and found to be compatible with a measurement using simulated $t\bar{t}$ events. However, a systematic uncertainty is assigned to cover the effect of possible residual differences by randomly rejecting jets based on the measured JRE.

Trigger, lepton identification efficiency, energy scale and resolution

The modelling in simulation of the lepton trigger, reconstruction and selection efficiencies as well as the energy resolution and scaling (e trigger, μ triggger, e recID, μ recID, e smearing, μ smearing, MC E res) have been assessed using $Z \to ee$ and $Z \to \mu\mu$ events.

Generator and parton shower dependence

The baseline generator MC@NLO+HERWIG may not correctly predict the kinematic distribution of $t\bar{t}$ events, which may result in differences in the acceptance and flavour composition of selected events. A systematic uncertainty is assigned to the choice of Monte Carlo generator (Generator) by comparing the results produced with the baseline $t\bar{t}$ generator with those produced with events simulated with POWHEG+HERWIG. Uncertainties in parton shower modeling (Fragmentation) are estimated by comparing results between event generated with POWHEG+HERWIG and those generated using POWHEG+PYTHIA.

Initial and final state radiation

Initial and final state radiation (IFSR) directly affects the flavour composition of the $t\bar{t}$ events. The associated systematic uncertainty due to IFSR is estimated by studies using samples generated with ACERMC [37] interfaced to PYTHIA, and by varying the parameters controlling ISR and FSR in a range consistent with experimental data [18].

Pileup

No explicit uncertainty is assigned to the effect of pileup as the Monte Carlo simulation is reweighted on an event by event basis to reproduce the distribution of the average number of primary vertices measured

in data. Uncertainties induced by pileup do indirectly enter the analysis through pileup-related uncertainties in object modeling such as the jet energy scale and missing transverse momentum corrections ($E_{\mathrm{T}}^{\mathrm{miss}}$ pileup).

Luminosity

The uncertainty in the integrated luminosity affects the measurement of the b-tagging efficiency due to the change in the overall normalisation of the backgrounds estimated from simulation. The integrated luminosity has been measured with a precision of 3.9% and is taken as a systematic uncertainty.

Summary

All individual contributions to the systematic uncertainties in bins of jet p_{T} are summarised in Tables 6 through 10 for the MV1 b-tagging algorithm at an operating point corresponding to an nominal efficiency of 70%. The systematic uncertainties are compared to the statistical uncertainty and the total uncertainty contribution to the scale factor is given. Whereas the total uncertainty of the tag counting and the kinematic selection methods are systematically dominated, the kinematic fit method is limited by data statistics.

p_{T}[GeV]	25-30	30-40	40-50	50-60	60-75	75-90	90-110	110-140	140-200	200-300
IFSR	±1.7	±2.5	±2.8	±3.1	±0.2	±0.2	±3.5	±0.4	±4.2	±7.9
Generator	±3.7	±2.7	±0.1	±0.6	±5.9	±0.6	±6.4	±1.6	±0.6	±1.0
Fragmentation	±2.3	±8.0	±2.9	±3.7	±2.9	±3.4	±2.4	±4.1	±3.5	±4.4
Diboson	±0.7	±0.4	±0.0	±0.1	±0.2	±0.3	±0.3	±0.7	±0.7	±0.1
Single top	±0.7	±0.5	±0.1	±0.3	±0.1	±0.2	±0.3	±0.8	±0.9	±0.4
Z + jets	±1.1	±0.4	±0.5	±0.3	±0.5	±0.3	±0.3	±0.5	±0.6	±0.7
W + jets	±1.6	±0.5	±0.5	±0.5	±0.4	±0.7	±0.5	±0.6	±0.5	±1.1
Multijet	±2.2	±0.8	±1.5	±1.6	±0.8	±1.8	±1.3	±1.4	±1.1	±1.4
JES	±3.2	±2.5	±1.7	±0.7	±1.5	±2.5	±2.2	±2.6	±2.7	±4.2
JER	±14.1	±9.8	±11.1	±3.8	±0.8	±1.4	±3.2	±4.0	±4.8	±4.2
JRE	±0.8	±0.5	±0.1	±0.2	±0.2	±0.0	±0.2	±0.3	±0.2	±0.1
JVF	±4.1	±0.6	±0.5	±0.2	±0.6	±0.5	±0.5	±0.6	±0.6	±1.5
W+HF SF	±0.9	±0.7	±0.2	±0.4	±0.3	±0.5	±0.4	±1.1	±1.0	±0.4
ε_c	±1.9	±1.3	±1.4	±1.3	±1.3	±1.2	±1.4	±1.1	±1.1	±1.5
ε_{light}	±3.8	±1.0	±0.8	±0.7	±0.9	±0.8	±0.6	±0.6	±0.5	±1.1
$E_{\mathrm{T}}^{\mathrm{miss}}$ cellout	±0.5	±0.4	±0.3	±0.5	±0.3	±0.4	±0.3	±0.6	±0.6	±0.1
$E_{\mathrm{T}}^{\mathrm{miss}}$ pileup	±0.5	±0.5	±0.4	±0.3	±0.4	±0.3	±0.4	±0.6	±0.5	±0.2
e trigger	±0.5	±0.5	±0.3	±0.3	±0.3	±0.4	±0.3	±0.6	±0.5	±0.5
e smearing	±0.4	±0.4	±0.5	±0.3	±0.1	±0.3	±0.4	±0.6	±0.7	±0.4
e recID	±1.0	±0.4	±0.5	±0.6	±0.5	±0.6	±0.5	±0.6	±0.6	±1.0
MC E res	±0.6	±0.5	±0.3	±0.2	±0.2	±0.3	±0.4	±0.6	±0.5	±0.3
μ trigger	±0.6	±0.6	±0.5	±0.5	±0.3	±0.4	±0.3	±0.5	±0.6	±0.8
μ smearing	±0.5	±0.4	±0.2	±0.4	±0.3	±0.3	±0.3	±0.5	±0.5	±0.4
μ recID	±0.7	±0.3	±0.2	±0.3	±0.3	±0.4	±0.3	±0.6	±0.6	±0.3
MC μ-en. sc.	±0.8	±0.4	±0.1	±0.2	±0.2	±0.6	±0.0	±0.7	±0.8	±0.1
Lumi	±1.7	±0.9	±0.9	±0.7	±0.6	±0.8	±0.9	±0.9	±1.2	±1.8
Stat.	±6.4	±4.0	±4.0	±4.0	±3.7	±4.4	±4.3	±4.6	±4.9	±5.4
Total Syst.	±27.2	±16.0	±13.0	±6.5	±7.8	±6.5	±9.9	±12.5	±10.4	±21.6
Total	±27.9	±16.5	±13.6	±7.6	±8.7	±7.8	±10.8	±13.3	±11.5	±22.2

Table 6: Uncertainties for the tag counting method in the single lepton channel (e+jet and μ+jet combined). The table shows relative uncertainties (in %) for the MV1 algorithm at an operating point corresponding to a 70% tagging efficiency.

p_{T}[GeV]	25-30	30-40	40-50	50-60	60-75	75-90	90-110	110-140	140-200	200-300
IFSR	±1.2	±2.2	±3.0	±5.7	±3.2	±2.0	±2.3	±1.6	±8.1	±13.6
Generator	±2.5	±0.7	±1.4	±1.9	±0.6	±0.1	±1.3	±5.9	±1.4	±7.4
Fragmentation	±6.3	±1.0	±5.0	±7.1	±4.7	±0.3	±1.2	±4.4	±2.2	±17.2
Diboson	±0.0	±0.2	±0.1	±0.2	±0.1	±0.1	±0.2	±0.1	±0.1	±0.5
Single top	±0.5	±0.5	±0.3	±0.5	±0.4	±0.3	±0.5	±0.5	±0.4	±0.8
Z + jets	±1.3	±1.2	±1.3	±1.3	±1.3	±1.3	±1.2	±1.3	±1.2	±1.0
Multijet	±1.4	±1.6	±1.7	±1.7	±1.9	±1.9	±1.9	±2.0	±2.0	±1.9
JES	±1.7	±1.7	±1.4	±1.2	±0.6	±1.2	±1.4	±1.6	±1.7	±1.8
JER	±4.1	±2.2	±0.6	±0.1	±1.0	±1.5	±1.1	±0.7	±1.5	±3.2
JRE	±0.0	±0.0	±0.2	±0.1	±0.1	±0.1	±0.3	±0.1	±0.1	±0.2
JVF	±0.6	±0.5	±0.5	±0.7	±0.5	±0.5	±0.6	±0.7	±0.7	±0.5
W+HF SF	±0.5	±0.5	±0.5	±0.5	±0.4	±0.5	±0.6	±0.5	±0.5	±0.8
ε_{c}	±0.7	±0.7	±0.5	±0.6	±0.5	±0.5	±0.6	±0.5	±0.6	±0.9
$\varepsilon_{\mathrm{light}}$	±1.0	±0.8	±0.8	±0.7	±0.6	±0.6	±0.5	±0.7	±0.8	±1.1
$E_{\mathrm{T}}^{\mathrm{miss}}$ cellout	±0.4	±0.7	±0.7	±0.4	±0.5	±0.6	±0.6	±0.5	±0.4	±0.8
$E_{\mathrm{T}}^{\mathrm{miss}}$ pileup	±0.6	±0.5	±0.6	±0.4	±0.5	±0.3	±0.6	±0.5	±0.5	±0.8
e trigger	±0.5	±0.6	±0.4	±0.6	±0.5	±0.5	±0.5	±0.6	±0.5	±0.7
e smearing	±0.5	±0.5	±0.5	±0.5	±0.4	±0.3	±0.5	±0.4	±0.6	±0.7
e recID	±0.5	±0.6	±0.6	±0.7	±0.6	±0.7	±0.8	±0.6	±0.7	±0.7
MC e-en. Scale	±0.5	±0.4	±0.6	±0.5	±0.5	±0.5	±0.6	±0.3	±0.6	±0.7
μ trigger	±0.5	±0.7	±0.6	±0.7	±0.7	±0.5	±0.5	±0.8	±0.4	±0.4
μ smearing	±0.6	±0.6	±0.6	±0.5	±0.6	±0.5	±0.5	±0.6	±0.7	±0.6
μ recID	±0.6	±0.4	±0.5	±0.5	±0.4	±0.4	±0.6	±0.5	±0.6	±0.8
MC μ-en. Scale	±0.3	±0.1	±0.1	±0.1	±0.1	±0.1	±0.1	±0.1	±0.3	±0.3
Lumi	±0.8	±0.8	±0.8	±0.7	±0.8	±0.8	±0.8	±0.8	±0.7	±0.6
Stat.	±4.9	±3.1	±2.9	±2.9	±2.6	±3.1	±3.1	±3.5	±4.7	±9.4
Total Syst.	±9.0	±5.4	±7.3	±10.1	±7.1	±5.1	±5.7	±9.2	±10.1	±23.8
Total	±10.3	±6.2	±7.9	±10.5	±7.5	±5.9	±6.5	±9.8	±11.2	±25.6

Table 7: Uncertainties for the tag counting method in the dilepton channel (ee, $\mu\mu$ and $e\mu$ combined). The table shows relative uncertainties (in %) for the MV1 algorithm at an operating point corresponding to a 70% tagging efficiency.

p_{T}[GeV]	25-30	30-40	40-50	50-60	60-75	75-90	90-110	110-140	140-200	200 – 300
IFSR	±4.3	±3.2	±2.7	±3.1	±3.6	±4.0	±3.6	±4.0	±5.2	±8.0
Generator	±0.5	±0.2	±0.0	±0.2	±0.3	±0.1	±0.6	±1.2	±1.9	±3.9
Fragmentation	±0.1	±1.0	±1.9	±1.1	±2.0	±1.1	±0.8	±0.7	±0.3	±2.9
Diboson	±0.0	±0.0	±0.0	±0.0	±0.0	±0.0	±0.0	±0.0	±0.0	±0.0
Single top	±0.0	±0.0	±0.0	±0.0	±0.0	±0.1	±0.1	±0.1	±0.1	±0.2
Z+jets	±0.1	±0.1	±0.1	±0.1	±0.2	±0.2	±0.2	±0.3	±0.4	±0.5
W+jets	±1.8	±1.5	±1.0	±0.8	±0.8	±0.8	±0.7	±0.7	±1.0	±1.3
Mulitjet	±1.5	±1.3	±1.4	±1.7	±1.6	±1.4	±1.6	±1.6	±1.9	±1.9
$t\bar{t}$	±1.0	±0.9	±0.8	±0.9	±0.9	±0.9	±1.0	±1.1	±1.4	±1.5
$\varepsilon_{\mathrm{fake}}$	±1.7	±0.4	±0.2	±0.4	±0.4	±0.4	±0.4	±0.5	±0.5	±0.4
JES	±5.7	±3.2	±2.2	±1.1	±0.8	±0.4	±0.6	±1.2	±1.2	±2.8
JER	±5.0	±0.2	±0.5	±1.4	±0.3	±0.8	±0.6	±0.6	±0.6	±0.7
JRE	±0.0	±0.0	±0.0	±0.0	±0.0	±0.1	±0.0	±0.0	±0.1	±0.0
JVF	±0.2	±0.3	±0.0	±0.0	±0.2	±0.1	±0.0	±0.0	±0.0	±0.4
W+HF SF	±0.2	±0.2	±0.2	±0.2	±0.3	±0.3	±0.4	±0.5	±0.7	±0.9
ε_{c}	±0.6	±0.4	±0.3	±0.3	±0.3	±0.4	±0.4	±0.4	±0.5	±0.7
$\varepsilon_{\mathrm{light}}$	±0.3	±0.3	±0.4	±0.4	±0.6	±0.7	±0.9	±1.1	±1.4	±2.0
$E_{\mathrm{T}}^{\mathrm{miss}}$ cellout	±0.1	±0.0	±0.0	±0.0	±0.0	±0.1	±0.0	±0.1	±0.0	±0.1
$E_{\mathrm{T}}^{\mathrm{miss}}$ pileup	±0.1	±0.0	±0.0	±0.0	±0.0	±0.0	±0.0	±0.0	±0.0	±0.1
e trigger	±0.0	±0.0	±0.0	±0.0	±0.0	±0.0	±0.0	±0.0	±0.0	±0.0
e smearing	±0.0	±0.0	±0.0	±0.0	±0.0	±0.0	±0.0	±0.0	±0.0	±0.0
e recID	±0.1	±0.0	±0.0	±0.0	±0.0	±0.0	±0.0	±0.0	±0.0	±0.0
MC E res	±0.0	±0.0	±0.0	±0.0	±0.0	±0.0	±0.0	±0.0	±0.1	±0.0
μ trigger	±0.0	±0.0	±0.0	±0.0	±0.1	±0.1	±0.1	±0.0	±0.1	±0.1
μ smearing	±0.0	±0.0	±0.0	±0.0	±0.0	±0.0	±0.0	±0.0	±0.0	±0.0
μ recID	±0.0	±0.0	±0.0	±0.0	±0.0	±0.0	±0.0	±0.0	±0.0	±0.0
Lumi	±0.2	±0.2	±0.0	±0.0	±0.0	±0.0	±0.1	±0.1	±0.1	±0.1
Stat.	±5.0	±3.0	±2.6	±2.4	±1.9	±2.0	±1.9	±2.1	±2.6	±5.1
Total Syst.	±9.4	±5.2	±4.4	±4.3	±4.8	±4.8	±4.6	±5.2	±6.6	±10.6
Total	±10.6	±6.0	±5.2	±4.9	±5.1	±5.2	±5.0	±5.6	±7.1	±11.8

Table 8: Uncertainties for the kinematic selection method in the single lepton channel (e+jets and μ+jets channels combined). The table shows relative uncertainties (in %) for the MV1 algorithm at an operating point corresponding to a 70% tagging efficiency.

p_{T}[GeV]	25-30	30-40	40-50	50-60	60-75	75-90	90-110	110-140	140-200	200-300
IFSR	±5.0	±4.0	±4.0	±4.2	±3.5	±3.8	±4.7	±4.7	±6.0	±9.2
Generator	±1.1	±0.7	±1.3	±1.0	±0.6	±2.1	±1.2	±0.5	±2.9	±8.1
Fragmentation	±2.7	±1.4	±1.7	±0.9	±1.1	±0.9	±0.3	±1.2	±1.2	±3.9
Diboson	±0.2	±0.1	±0.1	±0.1	±0.1	±0.0	±0.0	±0.0	±0.0	±0.0
Single top	±0.1	±0.1	±0.1	±0.0	±0.0	±0.0	±0.0	±0.0	±0.0	±0.1
Z + jets	±2.1	±1.7	±1.3	±1.1	±1.0	±1.1	±1.1	±1.5	±2.2	±4.7
$t\bar{t}$	±1.5	±0.9	±0.7	±0.6	±0.5	±0.6	±0.6	±0.6	±0.9	±1.0
JES	±8.3	±3.2	±2.0	±1.3	±0.3	±0.1	±0.3	±1.0	±1.3	±2.9
JER	±0.9	±1.1	±1.4	±0.3	±0.6	±0.1	±0.5	±0.1	±0.5	±0.5
JRE	±0.2	±0.0	±0.2	±0.0	±0.1	±0.0	±0.1	±0.1	±0.1	±0.2
JVF	±0.3	±0.3	±0.2	±0.1	±0.1	±0.0	±0.0	±0.1	±0.2	±0.2
W+HF SF	±0.2	±0.1	±0.1	±0.1	±0.1	±0.0	±0.0	±0.0	±0.0	±0.1
ε_{c}	±0.2	±0.1	±0.1	±0.1	±0.1	±0.1	±0.1	±0.1	±0.2	±0.5
$\varepsilon_{\mathrm{light}}$	±0.4	±0.2	±0.2	±0.1	±0.1	±0.1	±0.1	±0.1	±0.3	±1.1
$\varepsilon_{\mathrm{fake}}$	±1.2	±1.3	±0.8	±1.5	±0.9	±1.3	±1.1	±1.1	±0.9	±3.8
$E_{\mathrm{T}}^{\mathrm{miss}}$ cellout	±0.1	±0.1	±0.1	±0.1	±0.1	±0.0	±0.1	±0.1	±0.1	±0.2
$E_{\mathrm{T}}^{\mathrm{miss}}$ pileup	±0.1	±0.1	±0.1	±0.1	±0.1	±0.1	±0.1	±0.1	±0.1	±0.1
e trigger	±0.1	±0.1	±0.1	±0.0	±0.1	±0.0	±0.0	±0.1	±0.0	±0.1
e smearing	±0.1	±0.1	±0.1	±0.0	±0.0	±0.0	±0.0	±0.1	±0.0	±0.3
e recID	±0.1	±0.1	±0.1	±0.0	±0.1	±0.0	±0.1	±0.1	±0.0	±0.1
MC E res	±0.1	±0.1	±0.1	±0.1	±0.1	±0.0	±0.0	±0.1	±0.0	±0.2
μ trigger	±0.1	±0.1	±0.0	±0.0	±0.1	±0.0	±0.0	±0.1	±0.0	±0.1
μ smearing	±0.4	±0.2	±0.2	±0.2	±0.0	±0.2	±0.1	±0.3	±0.3	±1.4
μ recID	±0.1	±0.1	±0.1	±0.0	±0.0	±0.0	±0.0	±0.1	±0.0	±0.1
Fake lep.	±3.3	±1.1	±1.3	±1.3	±1.1	±1.3	±1.5	±1.0	±2.0	±0.4
Lumi ±3.9%	±0.3	±0.1	±0.1	±0.1	±0.1	±0.1	±0.1	±0.1	±0.2	±0.0
Stat.	±5.5	±3.2	±2.6	±2.6	±2.1	±2.4	±2.5	±2.9	±3.7	±10.7
Total Syst	±11.1	±6.1	±5.6	±5.2	±4.2	±5.0	±5.4	±5.6	±7.8	±15.1
Total	±12.3	±6.8	±6.1	±5.8	±4.7	±5.5	±5.9	±6.2	±8.5	±18.3

Table 9: Uncertainties for the kinematic selection method in the dilepton channel (ee, $\mu\mu$ and $e\mu$ combined). The table shows relative uncertainties (in %) for the MV1 algorithm at an operating point corresponding to a 70% tagging efficiency.

p_{T}[GeV]	25-30	30-40	40-50	50-60	60-75	75-90	90-110	110-140	140-200
IFSR	±1.8	±2.1	±2.1	±1.9	±2.5	±2.6	±2.2	±2.0	±1.8
Generator	±0.8	±0.3	±0.6	±1.7	±0.2	±0.4	±0.4	±0.9	±0.9
Fragmentation	±0.2	±0.4	±0.0	±0.4	±1.5	±0.3	±0.4	±2.0	±1.7
JES	±0.4	±0.7	±0.4	±1.2	±0.9	±0.4	±0.7	±2.1	±0.8
JER	±0.1	±0.0	±0.1	±0.1	±0.0	±0.0	±0.0	±0.0	±0.0
JRE	±0.2	±0.1	±0.0	±0.1	±0.0	±0.0	±0.0	±0.0	±0.0
$E_{\mathrm{T}}^{\mathrm{miss}}$ cellout	±0.4	±0.1	±0.2	±0.3	±0.1	±0.0	±0.1	±0.2	±0.3
$E_{\mathrm{T}}^{\mathrm{miss}}$ pileup	±1.2	±1.8	±1.2	±0.1	±0.6	±0.4	±2.2	±2.8	±0.6
e trigger	±0.1	±0.0	±0.0	±0.1	±0.0	±0.0	±0.0	±0.0	±0.0
e smearing	±0.1	±0.1	±0.1	±0.1	±0.0	±0.0	±0.0	±0.0	±0.0
e recID	±0.1	±0.1	±0.1	±0.1	±0.0	±0.0	±0.0	±0.0	±0.0
MC E res	±0.1	±0.1	±0.1	±0.1	±0.0	±0.0	±0.0	±0.0	±0.0
μ trigger	±0.1	±0.1	±0.0	±0.1	±0.0	±0.0	±0.0	±0.0	±0.0
μ smearing	±0.2	±0.1	±0.1	±0.1	±0.0	±0.0	±0.1	±0.0	±0.1
μ recID	±0.1	±0.1	±0.1	±0.1	±0.0	±0.0	±0.0	±0.0	±0.0
m_{top}	±1.4	±1.0	±1.2	±1.1	±0.4	±0.4	±0.6	±0.1	±1.1
χ^2 cut	±8.8	±17.4	±6.7	±9.8	±4.1	±11.1	±5.0	±6.4	±5.3
Pretag	±2.5	±2.9	±0.3	±1.3	±5.3	±4.9	±3.4	±2.6	±0.4
Stat.	±17.6	±10.1	±8.9	±9.3	±5.5	±7.7	±6.2	±6.3	±6.7
Total Syst.	±9.5	±17.9	±7.2	±10.4	±7.4	±12.5	±6.9	±8.3	±6.1
Total	±20.1	±20.6	±11.5	±13.9	±9.3	±14.6	±9.2	±10.4	±9.1

Table 10: Uncertainties for the kinematic fit method in the single lepton channel (e+jets and μ+jets channels combined). The table shows relative uncertainties (in %) for the MV1 algorithm at an operating point corresponding to a 70% tagging efficiency.

4.2 Measured b-tagging efficiencies and scale factors

The scale factors, including all systematic and statistical uncertainties, are summarised below. The scale factor and efficiencies for a representative operating point, corresponding to a b-tagging efficiency of 70%, of the MV1 tagger are presented in Figure 10 (single lepton) and Figure 11 (dilepton). The complete set of result for other tagging algorithms and operating points are listed in Tables 11 – 20.

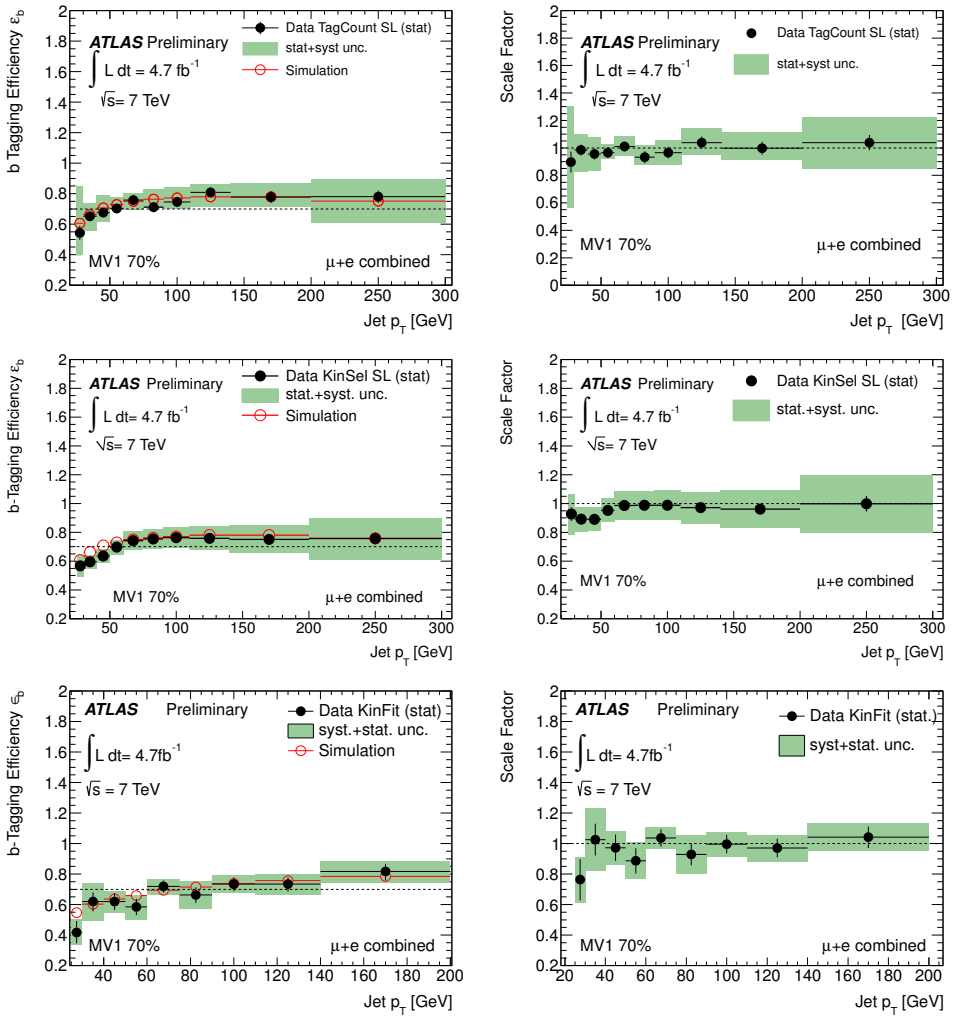

Figure 10: The measured b-tagging efficiency in data compared to that in simulation (left) and the resulting scale factors (right) for the MV1 algorithm at 70% b-tagging efficiency in the single lepton $t\bar{t}$ analyses. The results of all calibration methods (tag counting, kinematic selection and kinematic fit) are shown. The error bars show the statistical uncertainties while the green band indicates the total uncertainty.

p_T[GeV]	25-30	30-40	40-50	50-60	60-75
SV0 50 %	0.97±0.08	1.04±0.17	0.92±0.15	0.92±0.10	1.00±0.08
IP3D+SV1 60 %	1.01±0.08	0.97±0.14	0.96±0.14	1.01±0.07	0.98±0.08
IP3D+SV1 70 %	0.86±0.38	0.98±0.18	0.96±0.13	0.93±0.07	0.93±0.07
IP3D+SV1 80 %	1.04±0.34	0.99±0.25	0.95±0.17	0.91±0.07	0.93±0.07
JetFitterCOMBNN 57 %	0.84±0.73	1.05±0.14	0.94±0.12	0.96±0.06	0.99±0.08
JetFitterCOMBNN 60 %	0.82±0.62	1.04±0.12	0.97±0.12	1.00±0.06	1.00±0.08
JetFitterCOMBNN 70 %	0.90±0.34	1.00±0.16	0.96±0.13	1.01±0.06	1.01±0.09
JetFitterCOMBNN 80 %	1.01±0.28	0.98±0.17	0.98±0.14	0.94±0.06	1.01±0.08
MV1 60 %	1.06±0.08	1.02±0.15	0.94±0.12	1.00±0.06	1.01±0.09
MV1 70 %	0.90±0.34	0.98±0.16	0.96±0.13	0.96±0.06	1.01±0.08
MV1 75 %	0.85±0.30	0.99±0.19	0.96±0.13	0.96±0.06	0.96±0.08
MV1 85 %	1.14±0.26	1.00±0.17	1.02±0.15	0.92±0.07	0.97±0.07

Table 11: Scale factors for the tag counting method (25 GeV $< p_T <$ 75 GeV) in the single lepton channel (e+jets and μ+jets combined). The uncertainties are symmetrised and include the statistical uncertainty and all systematic uncertainties.

p_T[GeV]	75-90	90-110	110-140	140-200	200-300
SV0 50 %	1.00±0.09	0.96±0.10	1.05±0.12	0.97±0.12	0.97±0.23
IP3D+SV1 60 %	0.96±0.07	0.98±0.10	1.10±0.10	1.00±0.10	0.98±0.20
IP3D+SV1 70 %	1.01±0.06	0.98±0.08	1.05±0.10	1.01±0.10	1.13±0.21
IP3D+SV1 80 %	0.82±0.16	1.01±0.08	1.03±0.08	0.98±0.10	1.18±0.22
JetFitterCOMBNN 57 %	0.93±0.08	1.06±0.12	1.13±0.12	0.99±0.11	0.96±0.20
JetFitterCOMBNN 60 %	0.94±0.07	1.04±0.12	1.10±0.12	1.00±0.11	0.94±0.19
JetFitterCOMBNN 70 %	0.95±0.07	1.04±0.11	1.06±0.10	1.00±0.10	1.04±0.20
JetFitterCOMBNN 80 %	0.98±0.06	1.04±0.08	1.00±0.08	1.00±0.09	1.03±0.19
MV1 60 %	0.97±0.08	1.00±0.11	1.12±0.11	1.03±0.10	0.99±0.20
MV1 70 %	0.93±0.07	0.97±0.10	1.04±0.10	1.00±0.10	1.04±0.20
MV1 75 %	0.95±0.06	1.01±0.10	1.05±0.09	0.98±0.09	1.06±0.19
MV1 85 %	0.98±0.05	1.04±0.08	1.06±0.07	0.95±0.08	1.07±0.13

Table 12: Scale factors for the tag counting method (75 GeV $< p_T <$ 300 GeV) in the single lepton channel (e+jets and μ+jets combined). The uncertainties are symmetrised and include the statistical uncertainty and all systematic uncertainties.

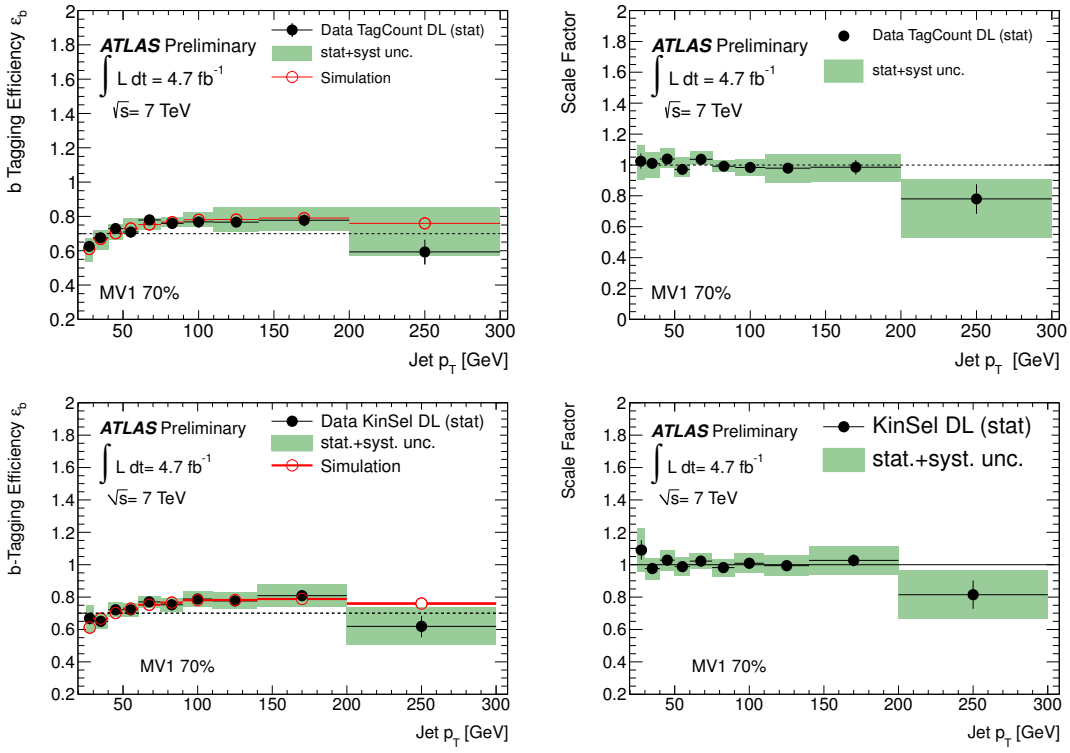

Figure 11: The measured b-tagging efficiency in data compared to that in simulation (left) and the resulting scale factors (right) for the MV1 algorithm at 70% b-tagging efficiency in the dilepton $t\bar{t}$ analyses. The results of both calibration methods (tag counting and kinematic selection) are shown. The error bars show the statistical uncertainties while the green band indicates the total uncertainty.

p_T[GeV]	25-30	30-40	40-50	50-60	60-75
SV0 50%	1.00±0.13	0.98±0.09	1.02±0.05	0.96±0.05	1.05±0.04
IP3D+SV1 60%	1.04±0.11	0.99±0.09	1.01±0.07	0.97±0.06	1.05±0.05
IP3D+SV1 70%	1.01±0.12	1.01±0.09	1.02±0.07	0.96±0.06	1.04±0.05
IP3D+SV1 80%	1.03±0.15	1.03±0.09	1.03±0.06	0.98±0.06	1.04±0.04
JetFitCOMBNN 57%	1.05±0.12	1.01±0.09	1.04±0.05	0.97±0.06	1.06±0.04
JetFitCOMBNN 60%	1.06±0.12	1.00±0.09	1.04±0.06	0.99±0.04	1.04±0.04
JetFitCOMBNN 70%	1.05±0.13	1.01±0.10	1.04±0.05	0.98±0.05	1.04±0.04
JetFitCOMBNN 80%	1.03±0.17	1.03±0.08	1.02±0.05	0.98±0.04	1.04±0.04
MV1 60%	1.01±0.11	1.01±0.09	1.03±0.06	0.98±0.05	1.04±0.04
MV1 70%	1.03±0.12	1.01±0.09	1.04±0.05	0.98±0.05	1.04±0.04
MV1 75%	1.03±0.14	1.02±0.09	1.03±0.05	0.97±0.05	1.04±0.04
MV1 85%	1.05±0.17	1.04±0.09	1.03±0.05	0.99±0.04	1.04±0.04

Table 13: Scale factors for the tag counting method (25 GeV $< p_T <$ 75 GeV) in the dilepton channel (ee, $\mu\mu$ and $e\mu$ combined). The uncertainties are symmetrised and include the statistical uncertainty and all systematic uncertainties.

p_T[GeV]	75-90	90-110	110-140	140-200	200-300
SV0 50%	1.00±0.05	0.96±0.06	0.96±0.10	1.00±0.11	0.78±0.26
IP3D+SV1 60%	1.00±0.05	0.98±0.05	0.95±0.10	0.99±0.12	0.77±0.26
IP3D+SV1 70%	1.00±0.05	0.98±0.06	0.96±0.10	0.99±0.12	0.81±0.22
IP3D+SV1 80%	1.00±0.05	0.99±0.06	0.96±0.10	0.98±0.13	0.86±0.18
JetFitCOMBNN 57%	1.03±0.04	0.99±0.08	0.97±0.10	1.00±0.11	0.85±0.27
JetFitCOMBNN 60%	1.03±0.05	1.00±0.09	0.96±0.10	1.01±0.10	0.82±0.26
JetFitCOMBNN 70%	1.02±0.05	0.99±0.05	0.97±0.10	0.98±0.10	0.78±0.37
JetFitCOMBNN 80%	1.00±0.05	0.99±0.05	0.97±0.09	1.00±0.10	0.82±0.19
MV1 60%	1.02±0.05	0.99±0.05	0.96±0.10	0.99±0.10	0.81±0.25
MV1 70%	0.99±0.04	0.99±0.05	0.98±0.10	0.99±0.10	0.79±0.24
MV1 75%	1.00±0.05	1.00±0.05	0.97±0.09	1.00±0.10	0.81±0.23
MV1 85%	1.02±0.05	0.99±0.05	0.97±0.09	1.00±0.09	0.87±0.13

Table 14: Scale factors for the tag counting method (75 GeV $< p_T <$ 300 GeV) in the dilepton channel (ee, $\mu\mu$ and $e\mu$ combined). The uncertainties are symmetrised and include the statistical uncertainty and all systematic uncertainties.

p_T[GeV]	25-30	30-40	40-50	50-60	60-75
SV0 50%	0.96 ± 0.18	0.93 ± 0.14	0.91 ± 0.13	0.96 ± 0.12	0.99 ± 0.10
IP3D+SV1 60%	0.95 ± 0.19	0.91 ± 0.16	0.89 ± 0.15	0.96 ± 0.15	0.97 ± 0.13
IP3D+SV1 70%	0.98 ± 0.23	0.92 ± 0.20	0.93 ± 0.17	0.99 ± 0.17	0.98 ± 0.15
IP3D+SV1 80%	0.98 ± 0.25	1.00 ± 0.21	0.99 ± 0.19	1.02 ± 0.17	1.02 ± 0.15
JetFitCOMBNN 57%	1.01 ± 0.19	0.96 ± 0.16	0.93 ± 0.14	1.00 ± 0.14	1.04 ± 0.12
JetFitCOMBNN 60%	0.99 ± 0.19	0.94 ± 0.16	0.93 ± 0.14	1.00 ± 0.14	1.03 ± 0.12
JetFitCOMBNN 70%	1.02 ± 0.21	0.95 ± 0.18	0.94 ± 0.16	0.99 ± 0.15	1.03 ± 0.14
JetFitCOMBNN 80 %	1.08 ± 0.24	1.01 ± 0.19	1.00 ± 0.17	1.06 ± 0.16	1.09 ± 0.14
MV1 60%	0.98 ± 0.18	0.93 ± 0.15	0.90 ± 0.14	0.96 ± 0.14	0.98 ± 0.12
MV1 70%	0.93 ± 0.21	0.89 ± 0.17	0.89 ± 0.15	0.95 ± 0.15	0.98 ± 0.13
MV1 75%	0.98 ± 0.23	0.92 ± 0.19	0.92 ± 0.16	0.99 ± 0.15	1.00 ± 0.14
MV1 85%	1.04 ± 0.23	1.02 ± 0.20	1.00 ± 0.17	1.07 ± 0.15	1.04 ± 0.14

Table 15: Scale factors for the kinematic selection method (25 GeV $< p_T <$ 75 GeV) in the single lepton channel (e+jets and μ+jets combined). The uncertainties are symmetrised and include the statistical uncertainty and all systematic uncertainties.

p_T[GeV]	75-90	90-110	110-140	140-200	200-300
SV0 50%	0.98 ± 0.09	1.01 ± 0.10	1.02 ± 0.11	0.99 ± 0.16	0.97 ± 0.32
IP3D+SV1 60%	0.98 ± 0.12	0.99 ± 0.13	0.99 ± 0.16	0.97 ± 0.24	0.94 ± 0.55
IP3D+SV1 70%	0.98 ± 0.14	1.02 ± 0.14	1.02 ± 0.17	1.00 ± 0.26	1.00 ± 0.54
IP3D+SV1 80%	1.01 ± 0.14	1.03 ± 0.14	1.02 ± 0.18	1.00 ± 0.26	1.01 ± 0.51
JetFitCOMBNN 57%	1.05 ± 0.12	1.07 ± 0.12	1.04 ± 0.14	1.00 ± 0.21	1.01 ± 0.47
JetFitCOMBNN 60%	1.05 ± 0.12	1.05 ± 0.12	1.03 ± 0.15	1.01 ± 0.22	1.00 ± 0.48
JetFitCOMBNN 70%	1.05 ± 0.13	1.05 ± 0.14	1.04 ± 0.16	1.04 ± 0.24	1.09 ± 0.49
JetFitCOMBNN 80 %	1.08 ± 0.13	1.09 ± 0.14	1.07 ± 0.17	1.11 ± 0.25	1.16 ± 0.51
MV1 60%	1.00 ± 0.11	1.02 ± 0.12	1.02 ± 0.14	0.99 ± 0.22	1.01 ± 0.46
MV1 70%	0.98 ± 0.12	0.98 ± 0.13	0.97 ± 0.15	0.97 ± 0.23	1.00 ± 0.48
MV1 75%	0.99 ± 0.13	0.99 ± 0.13	0.98 ± 0.16	0.98 ± 0.24	0.99 ± 0.49
MV1 85%	1.03 ± 0.13	1.05 ± 0.13	1.04 ± 0.17	1.04 ± 0.24	1.06 ± 0.44

Table 16: Scale factors for the kinematic selection method (75 GeV $< p_T <$ 300 GeV) in the single lepton channel (e+jets and μ+jets combined). The uncertainties are symmetrised and include the statistical uncertainty and all systematic uncertainties.

p_T[GeV]	25-30	30-40	40-50	50-60	60-75
SV0 50%	0.93 ± 0.14	0.95 ± 0.08	0.99 ± 0.07	0.97 ± 0.06	1.03 ± 0.05
IP3D+SV1 60%	0.99 ± 0.15	0.96 ± 0.08	0.98 ± 0.07	0.97 ± 0.06	1.02 ± 0.05
IP3D+SV1 70%	1.02 ± 0.13	0.97 ± 0.07	0.99 ± 0.06	0.94 ± 0.06	1.01 ± 0.05
IP3D+SV1 80%	1.02 ± 0.11	1.00 ± 0.06	1.00 ± 0.05	0.95 ± 0.05	0.99 ± 0.04
JetFitCOMBNN 57%	1.03 ± 0.15	0.97 ± 0.08	1.02 ± 0.08	0.97 ± 0.07	1.03 ± 0.06
JetFitCOMBNN 60%	1.05 ± 0.15	0.96 ± 0.07	1.01 ± 0.07	0.99 ± 0.07	1.01 ± 0.06
JetFitCOMBNN 70%	1.07 ± 0.13	0.96 ± 0.07	1.01 ± 0.06	0.97 ± 0.06	1.00 ± 0.05
JetFitCOMBNN 80%	1.03 ± 0.10	0.99 ± 0.06	0.99 ± 0.05	0.96 ± 0.05	1.00 ± 0.04
MV1 60%	0.99 ± 0.15	0.95 ± 0.08	1.01 ± 0.07	0.97 ± 0.06	1.01 ± 0.05
MV1 70%	1.04 ± 0.13	0.96 ± 0.07	1.01 ± 0.06	0.97 ± 0.06	1.01 ± 0.05
MV1 75%	1.06 ± 0.12	0.97 ± 0.06	1.01 ± 0.06	0.96 ± 0.06	1.01 ± 0.04
MV1 85%	1.03 ± 0.10	0.99 ± 0.05	0.99 ± 0.05	0.96 ± 0.05	1.00 ± 0.04

Table 17: Scale factors for the kinematic selection method (25 GeV $< p_T <$ 75 GeV) in the dilepton channel (ee, $\mu\mu$ and $e\mu$ combined). The uncertainties are symmetrised and include the statistical uncertainty and all systematic uncertainties.

p_T[GeV]	75-90	90-110	110-140	140-200	200-300
SV0 50%	0.96 ± 0.06	0.96 ± 0.06	0.96 ± 0.06	1.00 ± 0.09	0.80 ± 0.14
IP3D+SV1 60%	0.97 ± 0.06	0.98 ± 0.06	0.95 ± 0.06	0.98 ± 0.09	0.81 ± 0.15
IP3D+SV1 70%	0.97 ± 0.06	0.99 ± 0.06	0.95 ± 0.06	0.99 ± 0.09	0.80 ± 0.13
IP3D+SV1 80%	0.97 ± 0.05	1.00 ± 0.05	0.95 ± 0.05	0.97 ± 0.08	0.80 ± 0.13
JetFitCOMBNN 57%	0.99 ± 0.07	1.00 ± 0.07	0.96 ± 0.08	1.01 ± 0.10	0.91 ± 0.19
JetFitCOMBNN 60%	0.99 ± 0.06	1.00 ± 0.07	0.95 ± 0.07	1.00 ± 0.10	0.87 ± 0.18
JetFitCOMBNN 70%	0.99 ± 0.06	0.99 ± 0.06	0.96 ± 0.07	0.99 ± 0.09	0.80 ± 0.14
JetFitCOMBNN 80%	0.97 ± 0.05	0.99 ± 0.06	0.97 ± 0.06	0.99 ± 0.09	0.82 ± 0.14
MV1 60%	0.98 ± 0.06	0.99 ± 0.06	0.95 ± 0.07	0.98 ± 0.09	0.84 ± 0.17
MV1 70%	0.96 ± 0.06	0.98 ± 0.06	0.98 ± 0.06	0.99 ± 0.09	0.82 ± 0.15
MV1 75%	0.97 ± 0.05	1.00 ± 0.06	0.97 ± 0.06	1.00 ± 0.08	0.81 ± 0.14
MV1 85%	0.98 ± 0.05	0.99 ± 0.05	0.97 ± 0.05	0.99 ± 0.08	0.85 ± 0.12

Table 18: Scale factors for the kinematic selection method (75 GeV $< p_T <$ 300 GeV) in the dilepton channel (ee, $\mu\mu$ and $e\mu$ combined). The uncertainties are symmetrised and include the statistical uncertainty and all systematic uncertainties.

p_T[GeV]	25-30	30-40	40-50	50-60	60-75
SV0 50%	0.71±0.21	1.02±0.21	0.93±0.14	0.95±0.15	1.06±0.11
IP3D+SV1 60%	0.78±0.19	0.96±0.18	0.93±0.12	0.97±0.13	1.02±0.09
IP3D+SV1 70%	0.77±0.15	1.05±0.17	0.93±0.10	0.95±0.12	1.01±0.08
IP3D+SV1 80%	0.69±0.12	1.00±0.13	0.94±0.08	0.95±0.10	1.02±0.06
JetFitCOMBNN 57%	0.74±0.18	1.08±0.19	0.89±0.12	0.91±0.13	1.05±0.10
JetFitCOMBNN 60%	0.72±0.17	1.08±0.19	0.92±0.12	0.94±0.13	1.01±0.09
JetFitCOMBNN 70%	0.76±0.15	1.00±0.16	1.00±0.10	0.90±0.11	1.04±0.08
JetFitCOMBNN 80%	0.75±0.12	0.99±0.14	0.95±0.08	0.97±0.10	1.05±0.06
MV1 60%	0.70±0.17	1.02±0.18	0.97±0.12	0.92±0.13	1.06±0.09
MV1 70%	0.76±0.15	1.03±0.16	0.97±0.10	0.89±0.11	1.04±0.08
MV1 75%	0.77±0.14	1.04±0.15	0.95±0.09	0.94±0.11	1.02±0.07
MV1 85%	0.71±0.11	0.93±0.12	0.97±0.07	0.98±0.09	1.03±0.05

Table 19: Scale factors for the kinematic fit method (25 GeV $< p_T <$ 75 GeV) in the single lepton channel (e+jets and μ+jets combined). The uncertainties are symmetrised and include the statistical uncertainty and all systematic uncertainties.

p_T[GeV]	75-90	90-110	110-140	140-200
SV0 50%	0.94±0.15	1.01±0.11	1.03±0.12	0.99±0.13
IP3D+SV1 60%	0.86±0.12	0.94±0.09	1.00±0.11	1.04±0.11
IP3D+SV1 70%	0.90±0.12	0.96±0.08	0.97±0.09	1.00±0.09
IP3D+SV1 80%	0.91±0.10	0.92±0.07	0.97±0.08	1.04±0.08
JetFitCOMBNN 57%	1.02±0.16	0.99±0.10	1.06±0.13	1.02±0.13
JetFitCOMBNN 60%	0.99±0.15	0.97±0.10	1.04±0.12	0.99±0.12
JetFitCOMBNN 70%	0.91±0.12	0.99±0.08	1.02±0.10	1.03±0.10
JetFitCOMBNN 80%	0.95±0.12	0.97±0.07	1.00±0.09	1.04±0.08
MV1 60%	0.92±0.13	0.97±0.09	1.00±0.11	1.01±0.12
MV1 70%	0.93±0.13	1.00±0.08	0.97±0.09	1.04±0.09
MV1 75%	0.92±0.12	0.98±0.07	0.99±0.09	1.04±0.08
MV1 85%	0.96±0.11	1.02±0.06	1.04±0.08	1.05±0.06

Table 20: Scale factors for the kinematic fit method (75 GeV $< p_T <$ 200 GeV) in the single lepton channel (e+jets and μ+jets combined). The uncertainties are symmetrised and include the statistical uncertainty and all systematic uncertainties.

4.2.1 Comparison of all Methods

To demonstrate the compatibility of all methods, the results for the MV1 b-tagging algorithm at the operating point corresponding to an efficiency of 70%, as shown in Figures 10 and 11, are summarised in Figure 12. The result of the combination of the system8 and $p_{\mathrm{T}}^{\mathrm{rel}}$ based on a dijet sample [1] is also shown in the same figure. The individual $t\bar{t}$ based calibration methods, both between different selections (single lepton and dilepton) and between different calibration methods (tag counting, kinematic selection and kinematic fit), are consistent with each other within uncertainties. Furthermore all results are in good agreement with the earlier calibration methods based on dijets and extend the range of the scale factors in p_{T} up to 300 GeV.

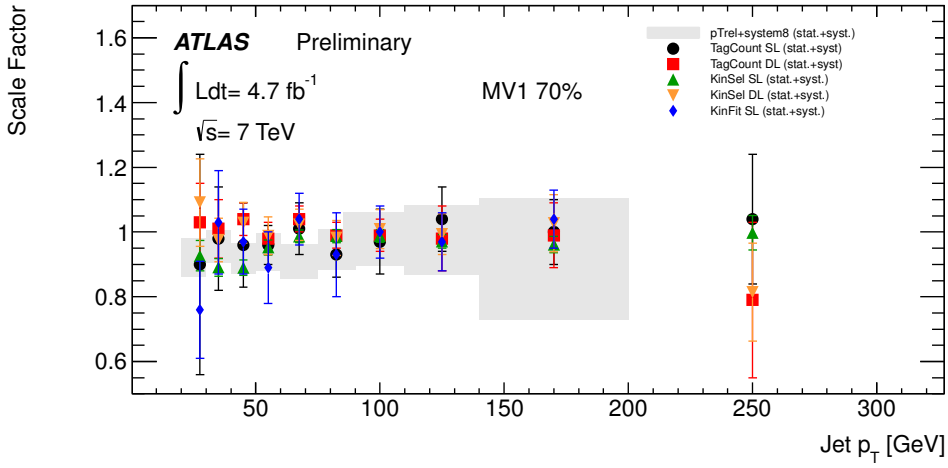

Figure 12: Comparison of all $t\bar{t}$-based scale factors with the combined scale factors from the system8 and $p_{\mathrm{T}}^{\mathrm{rel}}$ calibration methods based on dijet events. A high degree of compatibility is not only seen among the individual $t\bar{t}$ calibration methods but also between the $t\bar{t}$ and the other, totally independent, calibration methods.

5 Conclusion

Several methods based on $t\bar{t}$ single- and dilepton samples have been presented in this note to measure the b-tagging efficiency in data based for the b-tagging algorithms SV0, IP3D+SV1, JetFitterCombNN and MV1 for operating points corresponding to b-tagging efficiencies of 50% up to 85% in simulated $t\bar{t}$ events. The results are expressed in terms of scale factors, correcting the efficiencies in simulated events to those measured in data. For all b-tagging efficiencies, the scale factors measured with the different methods and samples are consistent with each other within uncertainties. Furthermore, good agreement with the b-tagging calibrations based on dijet samples has been demonstrated in Figure 12.

The b-tagging efficiency scale factors are close to unity for all values of jet p_{T} and η. The total uncertainties are ranging from 5% to 15% when subdividing the data into bins of jet p_{T}. With the integrated luminosity of 4.7 fb^{-1} collected in 2011, all $t\bar{t}$-based b-tagging efficiency measurements using the tag counting or kinematic selection methods are dominated by systematical uncertainties while the measurement using the kinematic fit method is statistics limited.

References

[1] The ATLAS Collaboration, *Calibrating the b-tag Efficiency and Mistag Rate in* $35\,pb^{-1}$ *of Data with the ATLAS Detector*, ATLAS-CONF-2011-089, June, 2011.

[2] The ATLAS Collaboration, *Statistical combination of top quark pair production cross-section measurements using dilepton, single-lepton, and all-hadronic final states at* $\sqrt{s} = 7$ TeV *with the ATLAS detector*, ATLAS-CONF-2012-024, March, 2012.

[3] S. Frixione and B. R. Webber, *The MC and NLO 3.4 Event Generator*, `arXiv:0812.0770`.

[4] M. Aliev et al., *HATHOR – HAdronic Top and Heavy quarks crOss section calculatoR*, Comput. Phys. Commun. **182** (2011) 1034–1046.

[5] A. Martin et al., *Parton distributions for the LHC*, Eur. Phy. J. **C63** (2009) 189–285.

[6] A. Martin et al., *Uncertainties on alpha(S) in global PDF analyses and implications for predicted hadronic cross sections*, Eur. Phy. J. **C64** (2009) 653–680.

[7] M. Cacciari et al., *Top-pair production at hadron colliders with next-to-next-to-leading logarithmic soft-gluon resummation*, Phys.Lett. **B710** (2012) 612–622.

[8] M. Czakon and A. Mitov, *Top++: a program for the calculation of the top-pair cross-section at hadron colliders*, `arXiv:1112.5675`.

[9] M. L. Mangano, M. Moretti, F. Piccinini, R. Pittau, and A. D. Polosa, *ALPGEN, a generator for hard multiparton processes in hadronic collisions*, JHEP **07** (2003) 001.

[10] J. Pumplin et al., *New generation of parton distributions with uncertainties from global QCD analysis*, JHEP **07** (2002) 012.

[11] Caravaglios, F. and Mangano, Michelangelo L. and Moretti, M. and Pittau, R., *A New approach to multijet calculations in hadron collisions*, Nucl.Phys. **B539** (1999) 215–232.

[12] P. Nason, *A new method for combining NLO QCD with shower Monte Carlo algorithms*, JHEP **11** (2004) 040.

[13] The ATLAS Collaboration, *The ATLAS Experiment at the CERN Large Hadron Collider*, JINST **3** (2008) S08003.

[14] M. Cacciari, G. P. Salam, and G. Soyez, *The anti-k(t) jet clustering algorithm*, JHEP **04** (2008) 063.

[15] M. Cacciari and G. P. Salam, *Dispelling the N**3 myth for the k(t) jet-finder*, Phys. Lett. **B641** (2006) 057.

[16] M. Cacciari, G. P. Salam, and G. Soyez. http://fastjet.fr/.

[17] The ATLAS Collaboration, *Probing the measurement of jet energies with the ATLAS detector using Z+jet events from proton-proton collisions at sqrt(s) = 7 TeV*, ATLAS-CONF-2012-053, May, 2012.

[18] The ATLAS Collaboration, *Expected performance of the ATLAS experiment: Detector, Trigger and Physics, Volume 1*, CERN-OPEN-2008-020, December, 2008.

[19] The ATLAS Collaboration, *Measurement of the charge asymmetry in top quark pair production in pp collisions at* $\sqrt{s} = 7$ *TeV using the ATLAS detector*, accepted for publication in EPJC, March, 2012. arXiv:1203.4211.

[20] T. A. Collaboration, *Measurement of the t-channel single top-quark production cross section in pp collisions at sqrt(s) = 7 TeV with the ATLAS detector*, Cern-ph-ep-2012-082, 2012. arXiv:hep-exp/1205.3130.

[21] The ATLAS Collaboration, *Measurement of the top pair production cross section in* pp *collisions at* $\sqrt{s} = 7$ TeV, Eur. Phy. J. **C71** (2011) 1577.

[22] The ATLAS Collaboration, *Calibrating the b-Tag Efficiency and Mistag Rate of the SV0 b-Tagging Algorithm in 3* pb^{-1} *of Data with the ATLAS Detector*, ATLAS-CONF-2010-099, November, 2010.

[23] The ATLAS Colaboration, *Commissioning of the ATLAS high-performance b-tagging algorithms in the* 7 TeV *collision data*, ATLAS-CONF-2011-102, July, 2011.

[24] The ATLAS Collaboration, *Measurement of the charge asymmetry in dileptonic decay of top quark pairs in pp collisions at s = 7 TeV using the ATLAS detector*, ATLAS-CONF-2012-057, Jun, 2012.

[25] The ATLAS Collaboration, *Measurement of the Mistag Rate of b-tagging algorithms with 5* fb^{-1} *of Data Collected by the ATLAS Detector*, ATLAS-CONF-2012-040, March, 2012.

[26] The ATLAS Collaboration, *b-jet tagging calibration on c-jets containing* D^+ *mesons*, ATLAS-CONF-2012-039, March, 2012.

[27] The ATLAS Collaboration, *Improved electron reconstruction in ATLAS using the Gaussian Sum Filter-based model for bremsstrahlung*, ATLAS-CONF-2012-047, May, 2012.

[28] R.K. Bock et al., *Formulae and methods in experimental data evaluation, with emphasis on high energy physics v.3*, Articles on statistical and numerical method, 1983.

[29] L. Lyons, *Statistics for nuclear and particle Physics*, Cambridge Univ. Press, 1986.

[30] J. D'Hondt et al., *Fitting of Event Topologies with External Kinematic Constraints in CMS*, CMS NOTE 2006/023, 2006.

[31] S. Moch and P. Uwer, *Heavy-quark pair production at two loops in QCD*, Nucl.Phys.Proc.Suppl. **183** (2008) 75–80.

[32] N. Kidonakis, *Two-loop soft anomalous dimensions for single top quark associated production with a W- or H-*, Phys.Rev. **D82** (2010) 054018.

[33] N. Kidonakis, *Next-to-next-to-leading-order collinear and soft gluon corrections for t-channel single top quark production*, Phys. Rev. D **83** (2011) 091503.

[34] N. Kidonakis, *Next-to-next-to-leading logarithm resummation for s-channel single top quark production*, Phys. Rev. D **81** (2010) 054028.

[35] J. M. Campbell, R. K. Ellis, and C. Williams, *Vector boson pair production at the LHC*, JHEP **1107** (2011) 018.

[36] The ATLAS Collaboration, *Measurement of the t-channel Single Top-Quark Production Cross Section in* $0.70 fb^{-1}$ *of* pp *Collisions at* $\sqrt{s} = 7$ TeV *collected with the ATLAS detector*, ATLAS-CONF-2011-101, July, 2011.

[37] B. P. Kersevan and E. Richter-Was, *The Monte Carlo event generator AcerMC version 2.0 with interfaces to PYTHIA 6.2 and HERWIG 6.5*, arXiv:hep-ph/0405247.